Modelling tyre vibrations
a modal approach

Blom, R.E.A.

Award date:
2005

Modelling tyre vibrations - a modal approach

DCT 2005.02

January 7, 2005
Eindhoven University of Technology (TU/e)

R.E.A. Blom s472444 (TU/e)

Supervisors: Prof. Dr. Ir. N.B. Roozen (TU/e)
Prof. Dr. H. Nijmeijer (TU/e)
Dr. Ir. I. Lopez Arteaga (TU/e)

Samenvatting

Geluid dat wordt veroorzaakt door autoverkeer is verantwoordelijk voor een groot deel van de geluidsoverlast. Een vermindering van het band/wegdek geluid zal de leefomstandigheden in gebieden vlakbij drukke wegen dus een stuk verbeteren. Een ander probleem is het interieurgeluid, het geluid dat door de inzittenden van het voertuig wordt gehoord. Ook hier is het band/wegdek geluid relatief belangrijker geworden doordat andere onderdelen, zoals de motor, stiller zijn geworden. Een vermindering van het band/wegdek geluid zal het comfortniveau in de auto dus verhogen. Om deze doelen te bereiken is het noodzakelijk om de mechanismen die verantwoordelijk zijn voor de geluidsopwekking te begrijpen en daardoor het onderzoek naar stillere band/wegdek combinaties die de veiligheid niet nadelig beïnvloeden mogelijk te maken. De vraag hiernaar is de drijvende kracht geweest achter onderzoek naar zowel het meten als het identificeren van de verschillende mechanismen, met als doel het reduceren van de geluidsproductie bij de bron. Ondanks deze inspanningen maakt de huidige kennis het voor de bandenfabrikanten nog steeds niet mogelijk om de geluidsproductie van een specifieke band/wegdek combinatie te voorspellen en zijn langdurige en dure proeven noodzakelijk bij het ontwerpen van een nieuwe band.

Dit verslag is dan ook gericht op het ontwikkelen van een model voor het voorspellen van band/wegdek geluid, waarbij de aandacht uitgaat naar geluid veroorzaakt door structurele opwekkingsmechanismen bij frequenties tussen de 50 en 1000 Hz. Vooral frequenties tot 500 Hz zijn belangrijk aangezien er geen modellen lijken te zijn die goede voorspellingen geven in dit gebied, dat overigens erg belangrijk is voor interieurgeluid. De mechanismen die belangrijk zijn in dit gebied zijn: 1) De globale vervorming die ontstaat in het contactvlak 2) Trillingen veroorzaakt door de profiel blokken die tegen de grond komen 3) Trillingen veroorzaakt door de ruwheid van het wegdek 4) Gordel resonanties. Aerodynamische mechanismen zijn niet belangrijk in dit frequentiegebied en worden dan ook buiten beschouwing gelaten.

Uit de literatuur blijkt dat alle analytische modellen ”uitgesmeerde” materiaaleigenschappen hebben die moeilijk te bepalen zijn. Bij de semi-analytische modellen is het lastig om het contact met het wegdek goed te beschrijven. Een volledig eindige elementen model kan de ingewikkelde opbouw en verschillende materialen van een band wel goed beschrijven, net als het contact met het wegdek. De rekentijden bij deze modellen zijn echter erg lang. Het bepalen van de eigenwaarden en -modes van een gedetailleerd eindige elementen model van een band om een modale basis op te spannen lijkt dan ook rekentechnisch een goedkope manier om de respons van een band te bepalen. Deze aanpak is verder onderzocht in dit verslag.

Uit de literatuur en een aantal numerieke experimenten is gebleken dat er twee belangrijke verschijnselen zijn die het model juist moet beschrijven: 1) De afname van de stijfheid in de buurt van het contactvlak door de verandering van de interne spanningen 2) De verschuiving van de dispersiecurves als gevolg van de rotatie. Het eerste punt wordt opgelost door de modes van de band te bepalen in de vervormde toestand. Het tweede door de stationaire rotatie van de band met een Euler aanpak te beschrijven.

Deze aanpak is getest, maar door problemen bij de post-processing van de door het eindige elementan pakket Abaqus berekende responsies kan geen goede vergelijking gemaakt worden. Echter de overige resultaten, dispersieplots en FRF's, leiden niet tot twijfels over deze aanpak. Deze resultaten komen overeen met resultaten uit de literatuur. Een nadeel van de aanpak die hier besproken wordt is dat er een groot aantal modes nodig is om juiste resultaten te verkrijgen. Tenslotte is een FE model van een bestaande band vergeleken met experimentele data, waaruit blijkt dat het FE model nog niet goed genoeg is voor dit doel.

Abstract

Noise generated by highway traffic is responsible for a substantial proportion of environmental noise pollution. Hence a reduction in tyre/road noise generation will greatly improve the roadside environment and the associated quality of life. Another concern is the interior noise, the noise that is heard by the occupants of the car. Again because of the reduction of e.g the engine noise, the tyre/road noise has become more important here and a reduction of this noise leads to a higher comfort level in the vehicle. To achieve these goals it is essential to understand the mechanisms of noise generation, and thereby facilitate the search for quiet tyre-tread/road surface combinations that do not compromise road safety. For over 30 years this requirement has driven extensive research in both measuring and identifying the tyre noise generation mechanisms, with the aim of reducing the noise at the source. In spite of these efforts, current knowledge still does not enable manufacturers to predict the noise emission of a specific tyre/road combination, and long and expensive tests are necessary for new tyre/road designs.

This master thesis is aimed at the development of a model for tyre-road noise, with a focus upon structure-borne noise radiation mechanisms at frequencies between 50 and 1000 Hz. More specifically frequencies up to 500 Hz, as it seems that there are no models that are able to give good predictions in this region, which is very important for interior noise. The mechanisms which are important in this frequency range are: 1) Running deflection 2) Tread impact 3) Texture impact 4) Belt resonances. Aerodynamical mechanisms do not seem to be important in the 50-1000 Hz range and are neglected.

A literature study points out that all analytical models have smeared out material properties, which are difficult to determine correctly. For the semi-analytical approaches it is difficult to describe the contact with the road. A full FE model on the other hand does include the detailed structure of the tyre and is able to describe the contact correctly. However the simulations take a very long time to complete. Therefore determining the eigenvalues and eigenmodes of a detailed FE-model of the tyre and then using these to construct a modal base of the tyre seems a computationally cheap way of calculating the time-domain response of the tyre. This approach is thus examined in this thesis.

The literature and a number of numerical experiments makes it clear that there are also two important phenomena that have to be described correctly by the model: 1) The decrease in stiffness near the contact patch due to the change in internal stress 2) The shift of the dispersion curves due to the rotation. The first is done by determining the modal base around the deformed state. The second is taken into account by describing the steady state rotation with an Eulerian approach.

This modelling approach is tested, but because of problems in post processing the calculated response from FE package Abaqus no satisfying comparison can be made. On the other hand the remaining results, the dispersion plots and FRF's, do not lead to doubts about this approach. These results agree with results from literature and therefore it is still thought to be correct. A drawback of the approach discussed in this thesis is that probably a large number of modes is needed to get accurate results. Finally a FE model of an actual tyre is compared to experimental data indicating that the FE model is not yet accurate enough for this purpose.

Contents

List of Symbols

Symbol	Definition	Unit
a	Radius	$[m]$
A	Rotation matrix	
c	Speed of sound	$[m/s]$
d_{cav}	Inner cavity diameter	$[m]$
d_{pipe}	Pipe diameter	$[m]$
$\vec{\mathbf{e}}^1$	Fixed reference coordinate system	[-]
$\vec{\mathbf{e}}^2$	Body fixed coordinate system	[-]
f	Frequency	$[Hz]$
$\mathbf{f}$	Excitation force vector	
g	Green's function	$[m/N]$
k,k_ϕ	Wave number	$[m^{-1}]$
k_a	Stiffness of the sidewalls and air pressure inside the tyre	$[N/m^2]$
k_T	Stiffness of the sidewalls and air pressure inside the tyre	$[N/m^2]$
q	Outside (driving) pressure in radial direction	$[N/m]$
m	Number half waves across the cross-section	[-]
n	Number of circumferential waves	[-]
$\mathbf{u}$	Displacement vector	
u_ϕ	Tangential displacement	$[m]$
u_r	Radial displacement	$[m]$
v_{veh}	Vehicle velocity	$[m/s]$
$\mathbf{z}$	Complex eigenvector	
B	Bending stiffness	$[Nm^2]$
$\mathbf{D}$	Damping matrix	
D_{cav}	Outer cavity diameter	$[m]$
E	Young's modulus of the tyre material	$[N/m^2]$
F	Driving force	$[N]$
$\mathbf{G}$	Gyroscopic matrix	
$\mathbf{H}$	Transfer function matrix	
$\mathbf{K}$	Stiffness matrix	
L_{cav}	Cavity length	$[m]$
L_{pipe}	Pipe length	$[m]$
$\mathbf{M}$	Mass matrix	
S	Cross-sectional area	$[m^2]$
t	Time	[s]
T_0	Tension	$[N]$
$\mathbf{V}$	Diagonal matrix containing eigenvalues	
$\mathbf{W}$	Inertial contribution to stiffness matrix	
$\hat{\mathbf{z}}$	Complex eigen column	

List of symbols continued...

Symbol	Definition	Unit
α	Angular position in the body fixed frame	[rad]
β	Angular position in the reference frame	[rad]
γ_1	Rayleigh damping coefficient (mass)	[-]
γ_2	Rayleigh damping coefficient (stiffness)	[-]
δ	Delta function	[-]
ζ	modal damping coefficient	[-]
$\boldsymbol{\eta}$	Modal displacement vector	
λ	Wave length, block length	$[m]$
λ	Eigenvalue	
$\vec{\phi}$	Eigenmode	
ξ	Displacement	$[m]$
ρ	Density of the tyre material	$[kg/m^3]$
ω	Frequency	$[rad/s]$
ω_n	Eigenfrequency	$[rad/s]$
$\mathbf{\Phi}^1_{bf}$	Matrix containing body fixed modes in reference coordinates	
$\mathbf{\Phi}^2_{bf}$	Matrix containing body fixed modes in body fixed coordinates	
$\mathbf{\Phi}^1_{rf}$	Matrix containing reference frame fixed modes in reference coordinates	
$\mathbf{\Phi}^2_{rf}$	Matrix containing reference frame fixed modes in body fixed coordinates	
Ω	Tyre rotational velocity	$[rad/s]$

Chapter 1

Introduction

Noise generated by highway traffic is responsible for a substantial proportion of environmental noise pollution. Vehicle noise is composed mainly of tyre/road noise and power unit noise. The cross-over speed, the speed where contributions of the tyre/road noise and power unit noise to the overall noise are about the same, is decreasing as time goes by. Thanks to modern technology, noise from passenger car engines and other mechanical parts has been significantly reduced. As a result, the tyre noise contribution has become more important even at moderate speeds. In the 1970's the cross-over speed was in the range of 50-70 kmh. Now tyre/road noise even dominates when driving 40 km/h at constant speed (see [Sandberg, 2001]). Hence a reduction in tyre/road noise generation will improve the roadside environment and the associated quality of life. Another concern is the interior noise, the noise that is heard by the occupants of the car. Again because of the reduction of e.g the engine noise, the tyre/road noise has become more important here and a reduction of this noise leads to a higher comfort level in the vehicle. To achieve these goals it is essential to understand the mechanisms of tyre/road noise generation, and thereby facilitate the search for quiet tyre-tread/road surface combinations that do not compromise road safety. For over 30 years this requirement has driven extensive research in both measuring and identifying the tyre noise generation mechanisms, with the aim of reducing the noise at the source. In spite of these efforts, current knowledge still does not enable manufacturers to predict the noise emission of a specific tyre/road combination, and long and expensive tests are necessary for new tyre/road designs. This is due to the number of different mechanisms involved in tyre noise generation and radiation, which often influence each other and which are dependent in a complex way on tyre and road design and operating conditions.

Tyre/road noise generation mechanisms can be divided into two groups:

- Vibrational mechanisms, mainly below 1000 Hz
- Aerodynamical mechanisms, mainly above 1000 Hz

This master thesis is aimed at the development of models for tyre-road noise, with a focus upon structure-borne noise radiation mechanisms at frequencies between 50 and 1000 Hz, and more specifically frequencies up to 500 Hz, as it seems that there are no models that are able to give good predictions in this region, which is very important for the interior noise.

The thesis starts with a short description of the noise generation mechanisms in chapter 2. To get a good idea of the modelling work that has been done in the past and is going on at the moment, a

literature study has been done. Because this thesis is focussed upon structure-borne noise, only vibrational models are discussed in this chapter. These models include 2D models, like Boehm's ring model [Boehm, 1966], as well 3D plate models e.g. the Chalmers model and shell models e.g. as in [Kim and Bolton, 2003]. Besides these analytical models also some numerical modelling is discussed. The results from this study are discussed in chapter 3. Then, in chapter 4, certain properties of a tyre are examined. For example the influence of rotation on the dynamics of the tyre.
In the next chapter, chapter 5, a new modelling approach is proposed. This is a modal approach and to take the influence of the contact with the road into account the modes are determined in the deformed situation. But this is only valid for a non-rotating tyre, so to take the effects of the rotation into account the steady state rotation is described by an Eulerian approach.
In chapter 6 an attempt is made to validate this modelling approach and a FE model of an actual tyre is compared to experimental data. Finally in chapter 7 the conclusions are discussed and recommendations are made.

Chapter 2

Generation mechanisms

The generation mechanisms of tyre/road noise have been investigated since the 1970's. This research has led to a complicated mix of mechanisms, all of which have some influence on the noise generation. In general, there is no disagreement among most experts on the existence of these mechanisms. However, the relative importance of these mechanisms is still disputed.

The most important mechanisms are discussed in this chapter. Also some phenomena closely related to the mechanisms are mentioned. These cannot be regarded as pure generation mechanisms, but they do influence the noise emission in a significant way. They are mentioned under the name "related amplification or reduction mechanisms". As mentioned in the introduction the mechanisms can be divided into two main groups:

1. Mechanisms related to vibrations of the tyre. These mechanisms mostly occur below 1000 Hz.
2. Mechanisms related to aerodynamical phenomena. These mechanisms mostly occur above 1000 Hz.

There is no simple answer to the question of which mechanism is the most important, since their relative contributions may vary for different tyres, roads and operating conditions.

The following sections will describe the mechanisms and the conditions under which they are important. The frequency ranges apply to "normal" tyres and "normal" surfaces. Much information is taken from [Sandberg and Ejsmont, 2002] to which the reader is referred for a more elaborate description of these mechanisms.

2.1 Vibrational mechanisms

2.1.1 Running deflection

As a tyre rotates it will be subject to a "running deflection" around its circumference, with the major forces acting at the trailing and leading edges of the contact patch. This momentary "distortion" and following forces in the radial direction will create forced and free vibrations which will propagate along the tread and also into the sidewalls.

2.1.2 Tread impact (300-1500 Hz)

The existence of a tread pattern with separate tread elements in the rolling direction causes a disruption of the smooth radial displacement at the contact patch edges. One could say that the tread elements impact or ”hammer” against the road surface, but since the road surface is non-compressible, the tread elements and the tread band will have to absorb the resulting deflection instead of the road. The tread pattern therefore induces vibrations in the tyre. The frequencies which are excited by this mechanism depend on the length of the tread blocks and the vehicle velocity.

$$f = \frac{v_{veh}}{\lambda} \tag{2.1}$$

where:
f : Frequency [Hz]
v_{veh} : vehicle velocity [m/s]
λ : block length [m]

2.1.3 Texture impact (800-1250 Hz)

This mechanism is basically the same as the tread impact mechanism. The difference is that now the surface texture is impacting against the tyre instead of the pattern block against the road. (2.1) is also valid for this mechanism, with λ being the distance between major asperities.

2.1.4 Stick/slip

When tread elements pass through the contact patch they accumulate a potential energy, until the forces exceed the friction forces. At this moment the block suddenly slips back to a position at which the friction forces are large enough to keep the block in place. This process is repeated many times per passage through the contact patch. This phenomenon only occurs when materials exhibit reduced friction with an increase in slip speed. Stick/slip as a generation mechanism is considered to be very important in situations where great tangential forces are applied to the tyre, such as during acceleration, braking or cornering. During free rolling or driving at constant speed this mechanism is considered to be much less important.

2.1.5 Stick/snap (above 1-2 kHz)

This mechanism occurs when a tyre becomes ”sticky” and the road surface is very clean. For example a ”winter” tyre at high temperature. The pattern blocks stick to the road surface and some force is needed to break the adhesion. Before the rubber releases from the surface the rubber will be stretched a little. When the block finally is released there will be some vibration in the rubber element to get back to its ”rest” position. The adhesion stick/snap mechanism is not considered to be very important for traffic noise, because the road surface is usually covered with a thin layer of dirt. The problem is however important for tyre tests on very clean drums in laboratories.

2.2 Aerodynamical mechanisms

2.2.1 Air turbulence (300 Hz)

The air around the tyre is put into motion by the rotation of the tyre. The noise which is generated by this mechanism only constitutes a significant contribution to tyre/road noise at speeds much higher than normal highway speeds. See [Hayden, 1971]. This means the mechanism is not important for the tyre road noise during speeds normally driven in traffic.

2.2.2 Air pumping (above 1000 Hz)

When a tyre rolls, a volume of air is enclosed in the contact patch within the cavities and pores constituted by the tread pattern grooves and surface texture. Air is compressed and pressed away at the front of the contact patch and expanded and sucked into the cavities at the rear. Even within the contact patch there will be significant air displacements. The variations of surface texture and tread pattern grooves, the latter of which will be rapidly squeezed, produce a variation of the air flow in time. This generates vibrations in the surrounding air and therefore constitutes a source of sound, characterised by the volume change per unit of time. Air pumping seems to be an important source of sound above 1000 Hz, especially on dense surfaces. On porous surfaces air pumping is less important because the air can escape from cavities more easily. Models to describe this phenomenon are discussed in [Hayden, 1971] and [Gagen, 1999].

2.2.3 Pipe resonances (900-2000 Hz)

In the contact patch pipes can be formed between the tyre tread pattern and the road surface. These pipes can either have both ends open or have just one open end. From basic acoustics it is known that the resonance frequencies for these pipes are:

Both ends open ($\lambda/2$-resonator)

$$f_n = \frac{nc}{2(L_{pipe} + 0.8d_{pipe})} \tag{2.2}$$

c : speed of sound [m/s]
n : integer
d_{pipe} : pipe diameter [m]
L_{pipe} : pipe length [m]
λ : wave length [m]

One end open ($\lambda/4$-resonator):

$$f_n = \frac{(n - 0.5)c}{2(L_{pipe} + 0.8d_{pipe})} \tag{2.3}$$

These pipe resonances then amplify air vibrations caused by for example the ”air pumping” mechanism. Just like air pumping the pipe resonances are more important in dense surfaces than on porous surfaces.

2.2.4 Helmholtz resonances (1-2.5 kHz)

A Helmholtz resonance occurs as an interaction in a simple mass-spring system. Applied to tyre noise generation, the volume of the cavity leaving contact with the road surface acts as a spring, and the air

present between the tread and the road acts as a mass. As the cavity moves out of the contact patch, a mass-spring system is suddenly created at the moment when the cavity opens to the air behind the tyre. Then, along with the cavity moving further away from the trailing edge, the volume and thus the mass of the air immediately outside the cavity will increase. Since the mass, spring and damping constants determine the resonance frequency, this frequency changes during the cavity movement; at the same time the resonance amplitude decreases. It means that there is a ”tone burst” associated with each cavity leaving the contact patch, starting at a high amplitude at a medium frequency and fading-off at a higher frequency.

2.3 Amplification/ reduction mechanisms

Besides the generation mechanism discussed in sections 2.1 and 2.2 there are some other phenomena which have an important influence on tyre/road noise. These mechanisms cannot be regarded as generation mechanisms though. The three most important of these mechanisms are discussed in the following sections.

2.3.1 Horn effect

Close to the leading and trailing edges of the tyre footprint, the tyre and the road surface form a structure with a narrow ”throat” at the edges, which widens more and more the further out from the edges one moves. This geometry provides a better match between the impedance at the ”throat” (where a major part of the noise is generated) and the ambient acoustical impedance.Graf determines the amplification due to the horn effect [Graf et al., 2002]. The amplification is determined relative to a situation without the tyre in place. Leading to the conclusion that amplifications due to the horn effect can reach up to 20 dB.

2.3.2 Torus cavity resonances (230-280 Hz)

The air column in the tyre cavity can resonate at a certain frequency. The frequency of the cavity resonance is defined only by the tyre and rim size and the speed of sound in the medium that inflates the tyre. A simplified equation for the cavity resonance frequency is:

$$f = \frac{c}{l_{cav}} = \frac{2nc}{\pi(D_{cav} + d_{cav})}[Hz] \tag{2.4}$$

c : speed of sound in the gas inflating the tyre [m/s]
l_{cav} : length of the cavity [m]
D_{cav} : outer diameter of the cavity [m]
d_{cav} : inner diameter of the cavity [m]
n : integer
Typical frequencies for passenger car tyres are in a range of 230-280 Hz (n=1), depending on the tyre size. This means this resonance is more important for interior noise than for exterior noise.

2.3.3 Belt resonances (600-1300 Hz)

The deformation of the tyre tread near the contact patch leads to radial and tangential stress discontinuities which induce vibrational modes in the carcass and the belt. The flexural waves propagate from the contact patch in both directions around the tyre, merge and create standing waves. According

to [Kim and Bolton, 2001] there are two types of waves: ”slow” (60-80 m/s) and ”fast” (180 m/s). See figure 2.1 The fast modes are considered to be efficient radiators.

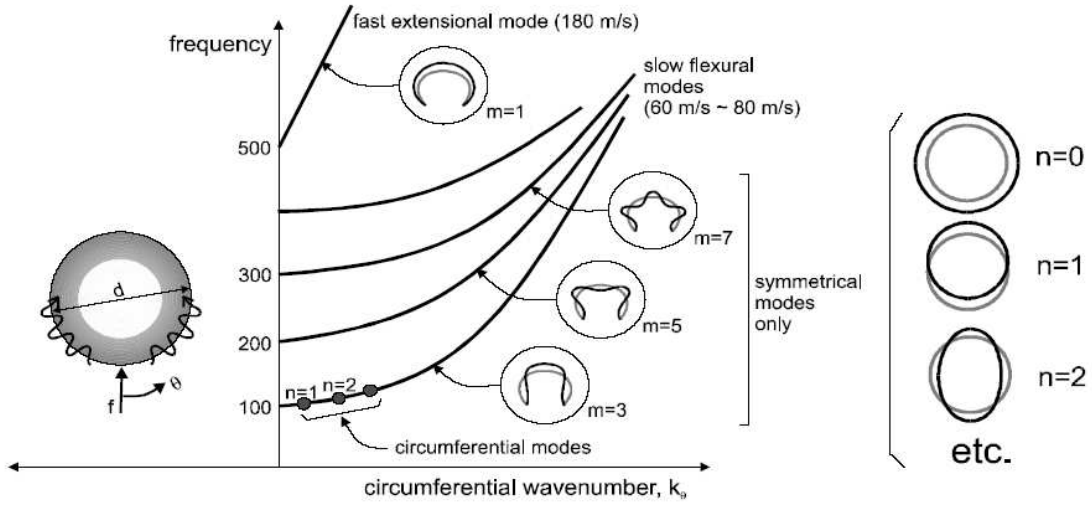

Figure 2.1: Typical tyre dispersion relations [Kim and Bolton, 2001]

2.4 Structure-borne noise

As mentioned in the introduction this thesis is focused on the development of a model for tyre/road noise with a focus upon structure-borne noise at frequencies between 50 and 1000Hz. In the previous sections it can be seen that the mechanisms which are important in this frequency range are:

1. Running deflection
2. Tread impact
3. Texture impact
4. Belt resonances

Aerodynamical mechanisms do not seem to be important in the 50-1000 Hz range and are neglected. This is more or less supported by a study done in [Kropp et al., 2003]. Figure 2.2 shows the contributions of the structure-borne and aerodynamical noise to the overall sound level. It can be seen that in the lower frequency range the structure-borne sound is the dominating source. In chapter 3 a literature study describing models, which try to describe one or more of the aforementioned vibrational mechanisms, is discussed.

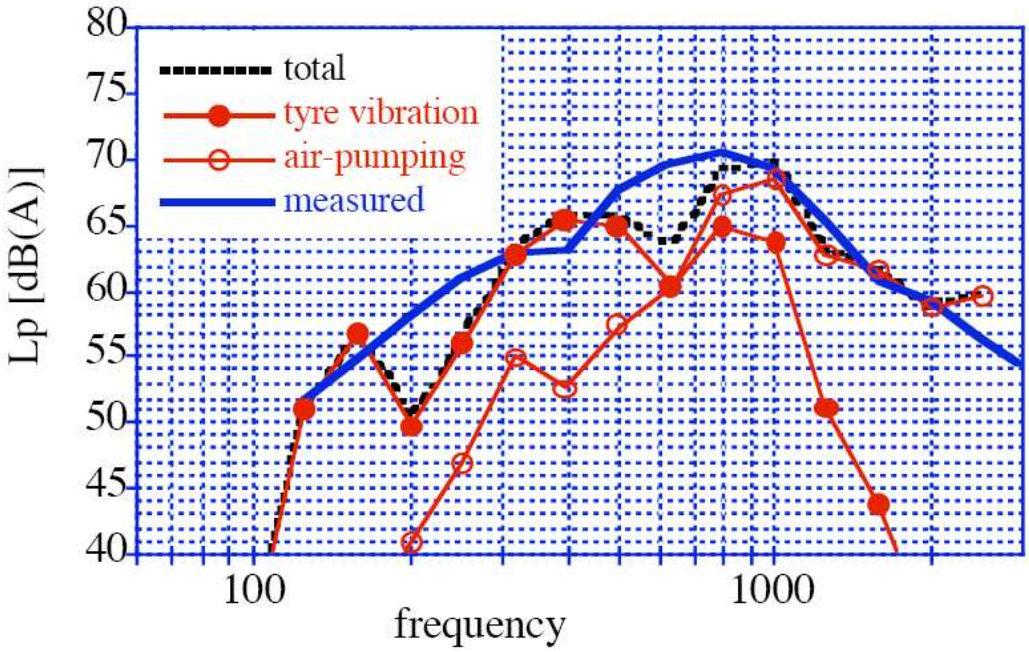

Figure 2.2: Contributions of the structure-borne and aerodynamical noise to the overall sound level [Kropp et al., 2003]

Chapter 3

Literature study

In this chapter the literature study concerning tyre models that describe tyre vibration is discussed. The models discussed vary from purely analytical models to purely finite element (FE) models. First the purely analytical models are discussed and then the combined analytical/numerical publications and semi-analytical approach are discussed. Finally the FE modelling is discussed.

3.1 Analytical models

In literature two types of analytical models can be distinguished. Models that do not consider modes with displacement variations across the treadband width (e.g. [Boehm, 1966], [Heckl, 1986] or [Kropp, 1989]) and models that do consider these modes. Therefore the first type of models (also called ring models) can only describe vibrations up to about 300 Hz. This is the frequency where the wavelength of the waves on the tyre is of about the same length as the tyre width. Therefore waves also start propagating in the cross-sectional direction of the tyre. The ring models are discussed first, after that the other models are discussed.

3.1.1 2D-Ring model (Boehm)

Most articles that use some kind of ring model use the model presented in [Boehm, 1966]. For example [Kropp, 1989] and [Heckl, 1986]. In these papers the following expressions for two-dimensional vibration are presented:

$$\frac{ES}{a^2}\left(\frac{\partial^2 u_\phi}{\partial^2 \varphi}+\frac{\partial u_r}{\partial \varphi}\right)-\frac{B}{a^4}\left(\frac{\partial^3 u_r}{\partial \varphi^3}+\frac{\partial u_r}{\partial \varphi}\right)=\rho S\frac{\partial^2 u_\phi}{\partial t^2}+k_T u_\phi \tag{3.1}$$

$$\frac{T_0}{a^2}\left(\frac{\partial^2 u_r}{\partial^2 \varphi}+u_\phi\right)-\frac{ES}{a^2}\left(\frac{\partial u_\phi}{\partial \varphi}+u_r\right)-\frac{B}{a^4}\left(\frac{\partial^4 u_r}{\partial \varphi^4}+\frac{\partial^2 u_r}{\partial \varphi^2}\right)=\rho S\frac{\partial^2 u_r}{\partial t^2}+k_a u_r-q \tag{3.2}$$

where:

- u_ϕ : tangential displacement $[m]$
- u_r : radial displacement $[m]$

- E : Young's modulus of the tyre material $[N/m^2]$
- S : cross-sectional area $[m^2]$
- a : radius $[m]$
- B : bending stiffness $[Nm^2]$
- ρ : density of the tyre material $[kg/m^3]$
- k_T : stiffness determined by elastic properties of the sidewalls and air pressure inside the tyre $[N/m^2]$
- T_0 : tension $[N]$
- k_a : stiffness determined by elastic properties of the sidewalls and air pressure inside the tyre $[N/m^2]$
- q : outside (driving) pressure in radial direction $[N/m]$

Apart from the problem that these models cannot account for displacement variations across the treadband width, the determination of the correct material parameters is also very difficult. This is because there are only a few parameters available to describe the tyre which is made out of dozens of materials and consists of many different layers. Apart from Boehm's model there are also some other, extended models. For example [Gong, 1993], where the Coriolis effect due to rotation of the tyre and two translational and one rotational degrees of freedom (DOF) of the wheel are taken into account. The latter makes it possible to study the vibration transmission properties of tyres under various constraint conditions and therefore can simulate the operation conditions of tyres on an automobile on actual road surfaces. However this model still has the two main problems of ring models, it is only valid in the range 0-300 Hz and it is difficult to determine the material parameters.

3.1.2 3D-Ring model

On of the disadvantages of the 2D ring models, the assumption that there are no displacement variations across the treadband, can be repaired by using more than one ring and interconnecting those rings by stiffnesses. This has been done in e.g. [Eichler, 1996]. This approach is also used in the software package FTire (see [FTire]). However this program is used for handling and comfort simulations (up to 120 Hz) and the problem remains how to determine the material parameters.

3.1.3 Chalmers-model (Kropp, Larsson et al.)

This model includes much more than just the vibrational properties of a tyre. However the radiation model is beyond the scope of this thesis and therefore this part of the model will not be discussed. The contact model used in this model on the other hand will be discussed.

Vibration Model

This well-known model basically describes a smooth tyre rolling at constant speed over a rough road surface. The most recent tyre model is based on the elastic field equations modelling a structure consisting of two coupled orthotropic layers under a static tension. The two layers represent the steel layer and the rubber tread. An elastic bedding supports the layers in all three directions to model the interior pressure of the tyre and contribution of the sidewalls stiffness (see figure 3.1). Since the contact between the tyre and the road is of non-linear nature the description of the vibrational properties of the tyre is formulated in the time domain. The circumference of the tyre is divided into discrete elements (slices with the width of the tyre), represented by their contact points. A matrix containing Green's functions (i.e. impulse response functions) describes the displacement response in any discrete point due to forces at these points. Main simplification of the model is the omission of the curvature of the real life structure, which leads to deviations at low frequencies (below 400 Hz, the ring frequency). However these deviations can be compensated for by for instance frequency dependent material data.

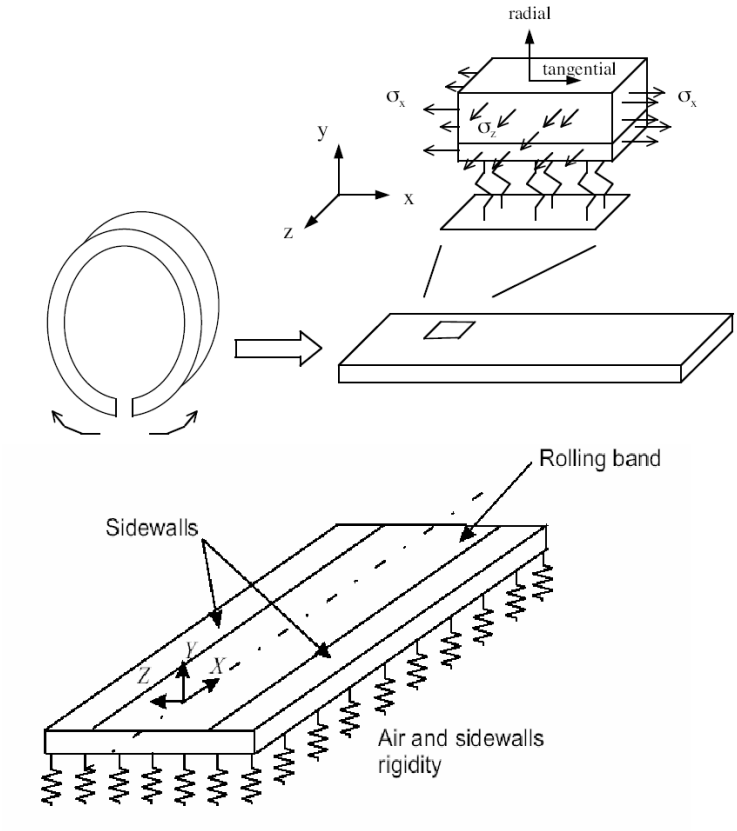

Figure 3.1: Schematic view of the Chalmers-model [Larsson and Kropp, 2002]

Contact model

The main idea is to describe the vibrational system (i.e. the tyre which is considered to be linear) by using an appropriate Green's function $g(t)$. As the excitation process is non-linear, it has to be described in the time-domain. The relation between driving force $F_m(t)$ and displacement $\xi_e(t)$ is

given by the convolution:

$$\xi_e(t) = \sum_m F_m(t) \times g_{m,e}(t) \tag{3.3}$$

where $g_{m,e}(t)$ is the Green's function representing the vibrational system with an input at the discrete point m and an output at the discrete point e. If there is more than one force acting the response of the system can be superposed (i.e. summation over m). The transition to a time discrete representation leads to:

$$\xi_e(N\Delta t) = \sum_m F_m(N\Delta t) g_{m,e}(0) + \sum_m \sum_{n=0}^{N-1} F_m(N\Delta t) g_{m,e}[(N-n)\Delta t] \tag{3.4}$$

As the local deformation of the tread is not considered in the Green's functions, the contact problem has to be solved in another way. At the moment two contact models are being used at Chalmers. Both will be discussed. The first contact model is an elastic foundation model (Winkler bedding) as described in Kropp [1999]. Assumptions made for the contactmodel are:

- Only when point e is in contact with the road a force F_e can act there.
- The amplitude of this force depends on the local deformation of the tread at this point.
- The force has to be seen as a function of the displacement of this point.

The tread is represented by massless uncoupled springs with the stiffness s_e at the discrete points. The contact force F_e is given by Hooke's law. Adhesive effects are neglected. Therefore a force only acts at these points, when the spring is compressed. $F_e(N\Delta t)$ is given by:

$$F_e(N\Delta t) = s_e \Delta y_e(N\Delta t) H[-\Delta y_e(N\Delta t)] \tag{3.5}$$

with

$$H(x) = \begin{cases} 0, & (\text{x}<0) \\ 1, & (\text{x}\geq 0) \end{cases} \tag{3.6}$$

where $\Delta y_e(N\Delta t)$ is the distance between point e on the tyre and the road surface. s_e is a function of the displacement $y_0(N\Delta t)$ of the centre of the rim, the position $k_{10}(\phi_e, N\Delta t)$ of point e when the belt is undeformed, displacement $x_e t$ of point e caused by the belt vibration and the roughness function $k_2(\phi_e)$ which describes the road.

$$\Delta y_e(N\Delta t) = y_0(N\Delta t) + k_{10}(\phi_e, N\Delta t) + \xi_e(N\Delta t) - k_2(\phi_e) \tag{3.7}$$

In (3.7) the assumption is made that before time $N\Delta t = 0$ the tyre has been at rest and it has not been in contact with the road.
In the second contact model an elastic half-space is used, described in [Wullens and Kropp, 2003]. The main difference between the elastic half-space and the Winkler bedding lies in the fact that in the elastic half-space the points are coupled with each other, while in the Winkler bedding a set of non-coupled springs is used. Because the points in the elastic half-space are coupled an iterative procedure is necessary to determine the displacements due to the roughnes profile at each time step. Therefore this model is computationally more expensive than the Winkler bedding.

Evaluation

In [Larsson and Kropp, 2002] the results from measurements and calculation are compared (figure 3.2).The agreement is much better for the tangential driving point mobility than for the radial driving point mobility. The discrepancy between measurements and calculations at low frequencies (below 400 Hz) is due to the curvature of the tyre being disregarded. Additionally, the resonance frequencies of the modes in the width direction are different for the calculation model and the real tyre. In the calculation model the stiffness is equal in both the x-direction (circumferential) and the z-direction (axial), while for a real tyre the stiffness varies in the different directions. Furthermore, the rim is considered as clamped in the calculation, which is hard to achieve in a real measurement situation. At higher frequencies the calculated mobility is increasing with higher frequency, while the measured one is almost constant. The reason for the rise in the calculated curve is the local stiffness

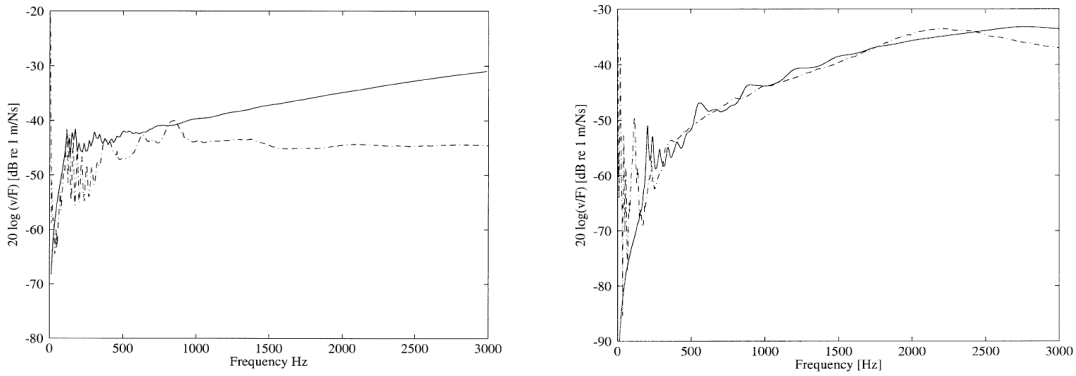

Figure 3.2: ***Left****: Calculated and measured radial driving point mobilities on the tyre. Solid line: calculation; Dashed line: measurement, [Larsson and Kropp, 2002].* ***Right****: Calculated and measured tangential driving point mobilities on the tyre. Solid line: calculation; Dashed line: measurement, [Larsson and Kropp, 2002].*

of the tread surface, due to a too low value of the shear modulus in the upper tread layer. The calculated radial mobility shows better agreement when the shear modulus of the upper layer is increased. However, for the tangential driving point mobility, the agreement with the measurement is poorer in this case. The fist resonance in the measurement of the tangential mobility corresponds to a rotation mode where the complete tyre rotates back and forth against the rim as a rigid body mode. This mode is not included in the calculation, which explains the discrepancy at low frequencies. The measurements also indicate that the damping is higher in the real tyre than that used in the calculation. The peaks are smoother and less visible in the measurements than in the calculations. To achieve a better agreement the material parameters have to be adapted to measurements on real tyres. The largest source of uncertainty in the calculation is the material data for the two-layer model. The data found in the literature are often given as an average value of the tyre cross-section, e.g., bending stiffness and density. In the suggested model, the material data have to be given to each layer individually. Some of the parameters are simple to obtain like, for instance, the thickness, but most data are difficult to establish or measure, especially with respect to the complex structure of the steel layers.

Current & Future work

- Determining the correct material parameters for each layer

3.1.4 A wave model for a pneumatic tyre belt [Pinnington & Briscoe, 2002]

Model

This model is presented in [Pinnington and Briscoe, 2002] and extended in [Pinnington, 2002]. First the basic model from the first article is discussed and then the extension from the second article. In [Pinnington and Briscoe, 2002] the tyre belt is represented as a tensioned Timoshenko beam upon an arbitrary sidewall impedance which means that the upper frequency is limited by the resonances across the belt thickness. In practical terms, this limit would be the first shear resonance of the tread blocks. The tyre is flattened like a snakeskin and is of infinite extent in the x-direction (circumferential, see figure 3.3). This approach is thought to be most appropriate at high frequencies when the damping inhibits modal behaviour and the sound radiation is most significant from the vibration local to the contact patch. It would not, in principle, be difficult to fit the boundary conditions of a ring to give the lower frequency modes if required, once the various wave types have been identified. However the results are only valid above the ring frequency, as curvature is not included in this model. In reality out-of-plane (radial) motion of the belt is associated with two types of sidewall motion:

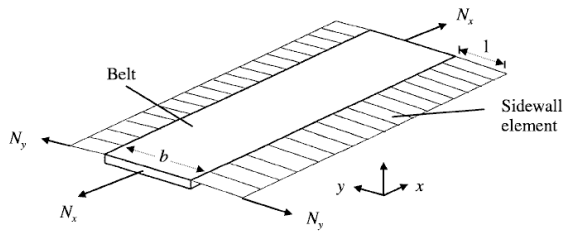

Figure 3.3: Belt and sidewall model [Pinnington and Briscoe, 2002]

stretching and flexure. In-plane stretching of the sidewall around the cross-section results in a change in cross-sectional area and couples this mode of carcass vibration to the air space within the tyre (see figure 3.4b). These breathing waves are important when considering transmission of force to the hub. The sidewall flexural motion (see figure 3.4a) is more noticeable than the stretching motion, although these cause a negligible change in cross-sectional area because of the cancellation effect of the opposing motion of half-wavelengths around the section. The structural waves are therefore not well coupled to the air space. Only waves associated with the flexural motion of the sidewall are considered here. In [Pinnington, 2002] a more physical model for the sidewalls is presented in two parts:

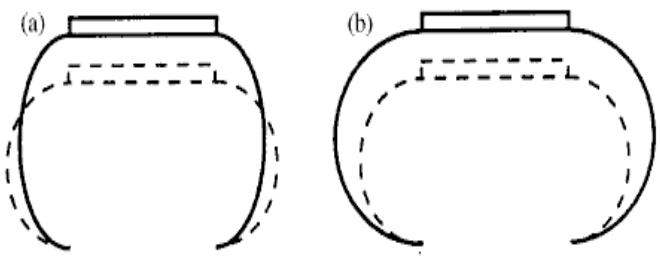

Figure 3.4: Cross-sectional deformation patterns of (a) bending and (b) stretching [Pinnington, 2002]

below the ring frequency (about 400 Hz) of the sidewall there is a ”static” model of a pressurized inextensible curved membrane under tension; above the ring frequency, there is a ”dynamic model” of a beam transmitting tension, bending and compression waves. The problem is divided in this manner about the ring frequency to simplify the analysis. At low frequencies in the regime of the ”static” model the sidewall and enclosed air transmit forces to the hub in two modes.
The first regards the sidewall as inextensible (a in figure 3.4), when radially inward motion of the belt is accompanied by sidewall bulging, which conserves the enclosed air volume and causes no coupling to the toroidal acoustic space. The second is the breathing mode of the tyre section (b in figure 3.4), involving stretching of the sidewall and consequent coupling with the air space within. The sidewall is much softer in the first mechanism described and so this tends to dominate over most of the frequency range. The second mechanism is thought to be only important for the excitation of the tyre acoustic cavity mode at about 250 Hz for passenger cars, when the cavity circumference is equal to an acoustic wavelength. Only the first mechanism, where the sidewall is inextensible, is considered here in the ”static” model. At frequencies greater than the ring frequency the curvature of the sidewall can be neglected, and the out-of-plane and axial deformations regarded separately.

Evaluation of the model

It is difficult to compare the measured and calculated responses that are presented in the paper. Therefore it is very difficult to tell how accurate the model is. However some general remarks can be made following from the assumptions and simplifications made in this model.
First of all, the curvature is neglected in this model also; this means that the model is only valid above the ring frequency (about 400 Hz). Secondly the belt is considered to be of infinite length, therefore no belt resonances will occur in the model. Furthermore the in-plane stretching of the sidewalls is also not considered. Another problem is which material parameters to use, as a tyre is made out of al lot of different layers. This means ”smeared” material parameters have to be used. Finally, the upper limit of the frequency is limited by the resonances across the belt depth. In practical terms, this would be the first shear resonance of the tread blocks.

Current & Future work

- In-plane stretching of the sidewall

3.1.5 An orthotropic two-plate wave model [Muggleton et al. 2003]

Model

In this model the primary propagation direction is considered to be across the tyre, whilst variation in the circumferential direction is accounted for by decomposing the response into harmonic components around the tyre. The system is modelled as an idealization of a tyre. The tread and sidewalls are each modelled as a thin, flat orthotropic plate, with in-plane tension, which arises as a result of the internal pressure in the tyre. Tread curvature is ignored so that the tyre is effectively ”unwrapped” circumferentially, and continuity of displacement and slope is applied at the ends to reflect the fact that they are, in fact, joined. The plates are assumed to vibrate in bending (flexural) and in-plane motion is neglected. To represent the longitudinal (in-plane) stiffness of the sidewall, it is joined to the tread via a translational stiffness as shown in figure 3.5, with continuity of slope being preserved between the two tyre elements. The stiffness arises primarily from the curvature induced by the internal pressure and also from a combination of axial stretching, bending and shear deformation. The sidewall is

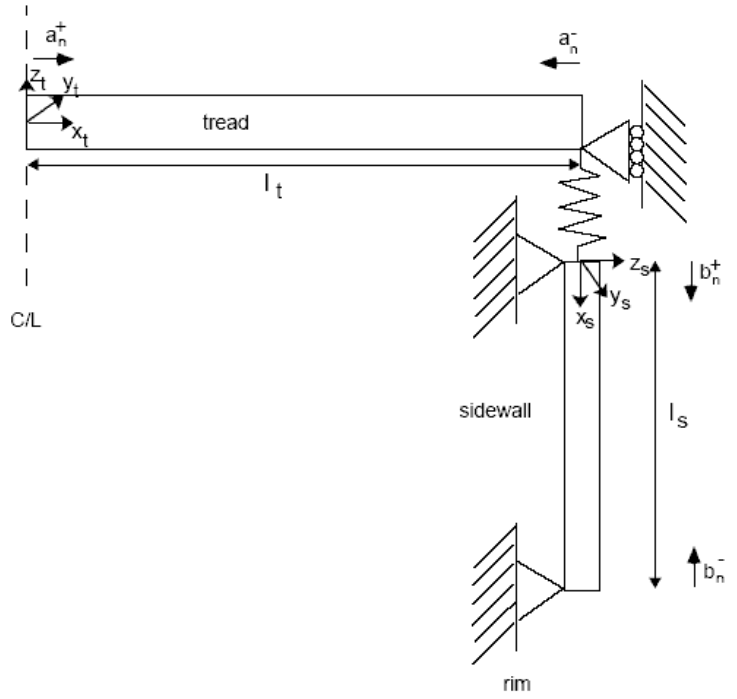

Figure 3.5: Representation of the cross-section of the tyre. [Muggleton et al., 2003]

connected to the rim by a simple support, which is assumed to be rigid. Excitation is a constant line force applied along a short length of the centreline of the tyre. A wave approach is used to model the behaviour of the system, and the dynamic response is found by summing contributions from a number of wave components. Waves are injected into the system by the force and travel through it, being reflected and transmitted at the joint between the tread and the sidewall, and again being reflected at the sidewall/rim joint.

Evaluation of the model

As can be seen in figures 3.6- 3.8 there is a big difference between the measured responses and the calculated responses. However the model seems able to predict the qualitative behaviour accurately. The first resonance is associated with ”tread bounce”, in which the tread moves predominantly as a rigid mass on the sidewall stiffness. Then there follows a set of resonances associated with higher order circumferential modes with the same basic cross-wise motion. At higher frequencies, further groups of circumferential resonances cut on, each with its own characteristic cross-wise response. At high frequencies, the response tends towards that of a point-excited infinite orthotropic plate, limited by the finite length of the excitation line.

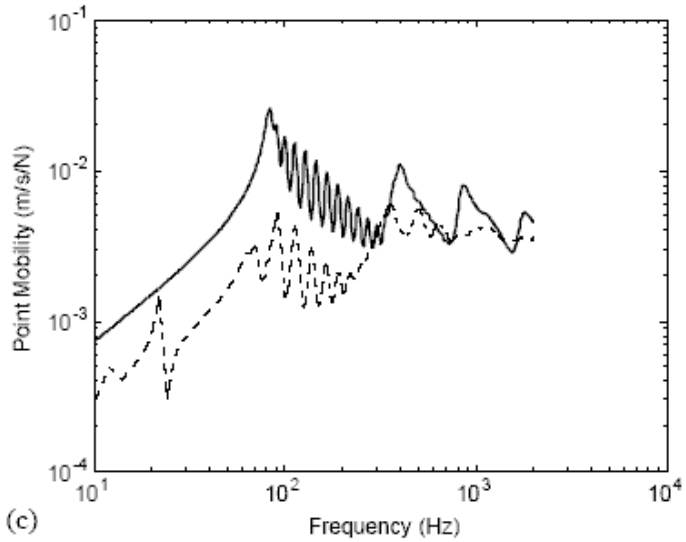

Figure 3.6: Measured (dashed) and calculated (solid) point mobility. [Muggleton et al., 2003]

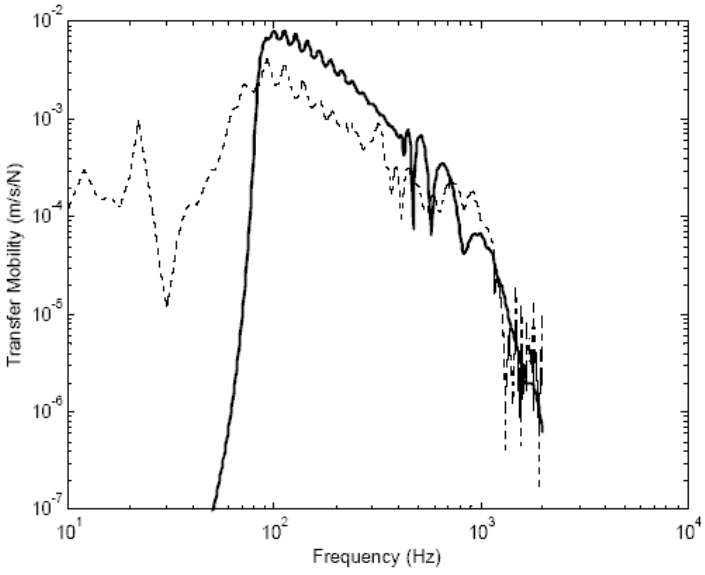

Figure 3.7: Measured (dashed) and calculated (solid) transfer mobility. [Muggleton et al., 2003]

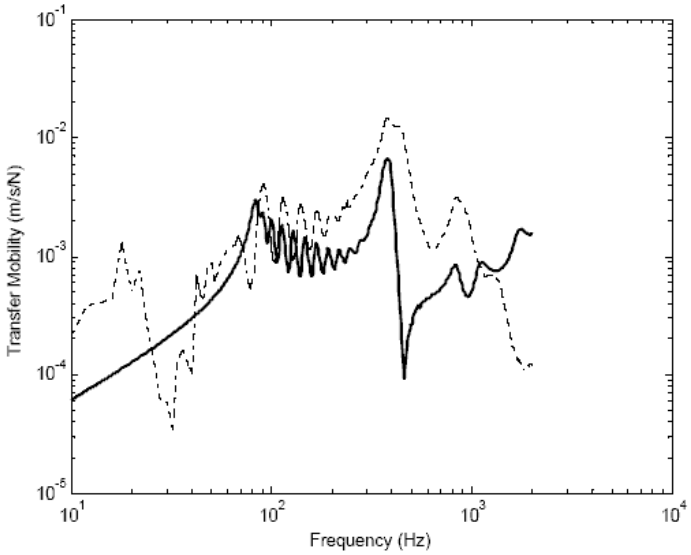

Figure 3.8: Measured (dashed) and calculated (solid) transfer mobility to sidewall [Muggleton et al., 2003]

According to [Muggleton et al., 2003] the large difference between measured and calculated responses are partly because of the uncertainty over the values for the elastic properties used in the model. Again, the model parameters are difficult to determine due to the complexity of the tyre. However some remarks still have to be made. According to literature, (e.g. [Larsson and Kropp, 2002] and [Pinnington and Briscoe, 2002]), simplifying the model by neglecting the curvature of the tyre makes the model valid only for frequencies above the ring frequency (about 400 Hz). Muggleton does not mention this constraint. Furthermore the top of the sidewall is connected to a simple support, which is assumed to be rigid (just like the rim side of the sidewall). In reality the topside of the sidewall is able to move in radial and tangential directions. However, according to [Muggleton et al., 2003] both issues (and other refinements) are subject of current and future work.

Current & Future work

- Including effects of in-plane motion
- Including effects of curvature
- Improvements to the description of the tread/sidewall junction
- Inclusion of non-uniform properties such as thickness and layer construction
- Inclusion of a non-rigid rim
- Extending the model to cope with excitation which is distributed across the tread

3.1.6 Elastic cylinder [O'Boy, 2004]

Model

At the time of writing a PhD-student of the Energy Group (prof. Ann P. Dowling) at the Department of Engineering of the University of Cambridge is also working on a model to predict tyre-noise. O'Boy [O'Boy, 2004a] describes how the surface vibration of an infinitely long elastic cylinder can be determined. Different layers, air pressure and damping are all taken into account. However, in order to accurately model and simulate the vibration of an automotive tyre, several development stages must be undertaken. The ultimate aim is to develop an accurate tyre model, detailing the surface vibration, in order to determine the far field noise produced. The inputs to this model should, where possible, utilise common engineering material properties, as used in the design stages of tyre companies. The model should allow experimental designs to be tested for noise production, to allow commercial trade offs to take place involving parameters such as cost, durability, grip, vehicle ride quality and handling, noise, water dispersion and vehicle vibration transmission. However to calculate the response using the cylinder model takes a long time. Therefore a fast running bending plate model is used, with parameters tuned to match the cylinder model, over a range of frequencies, axial wavelengths and angular orders.

Evaluation

No validation measurements were done in [O'Boy, 2004b] so it is not possible to give a meaningful evaluation at this time.

Current & Future work

- Validation of surface displacements.

3.2 Combined analytical/numerical and semi-analytical approaches

3.2.1 Early usage of shell models

One of the first publications in which the tyre is treated as a 3-dimensional object is [Soedel, 1975]. Here the tyre is viewed as an equivalent thin shell. The response of the rolling tyre is formulated by way of a three-dimensional Green function. This function can be formulated by using modal expansion. The mode shapes of complete shells of revolution with axisymmetric properties are known a priori (see figure 2.1). Therefore only the frequencies and amplitudes of these modes need to be obtained theoretically or experimentally. This leads subsequently to the general solution for any kind of tyre loading in terms of an integral. The integral may be simplified by expressing the loading on the tyre by its vector resultant. This approximation eliminates the need to obtain the exact load distribution in the tyre contact area. Introducing a modal damping factor for each natural mode can also include damping. This approach can handle frequencies up to 2000 Hz, depending on how well one is able to determine natural frequencies and modes. One advantage of this approach is that once the modes and natural frequencies have been determined, different loading conditions can be applied. This also makes it possible to determine the eigenfrequencies and natural modes with a large FE model containing all material properties, which should still be a relatively fast calculation, while the dynamic response to a certain input is then determined using the shell approximation. This way it is not necessary to determine parameters like the ones used in the ring model. (Bending stiffness,

stiffness of the sidewalls). Of course to be able to determine the eigenfrequencies and natural modes accurately using a FE model, one has to be able to describe the materials used in the tyre well. Main drawback of this approach is that it is a linear approach and does not include the contact problem. The modes of the shell are determined in the undeformed (not in ground contact) case. The ground contact, however, influences the modal behaviour of the tyre (see chapter 4), which invalidates the above mentioned approach.

A possible solution for the contact problem involving shells is presented in [Tielking and Schapery, 1981]. The contact solution procedure begins with the calculation of a sequence of transfer function matrices, which contains the response of the inflated shell to a sequence of harmonic ring loads applied on the finite element nodes (however the method is not restricted to finite elements according to [Tielking and Schapery, 1981]). The discrete Fourier transform (DFT) is then employed, with the transfer function matrices, to calculate an influence coefficient matrix that can be used to determine the response of the inflated toroid to an arbitrary array of point loads on each of the finite element nodes. A collocation procedure is used to establish the contact boundary and the distribution of point loads that arises with flat surface contact at the specified load radius.

[Keltie, 1982] uses a shell model to determine sound radiation by the surface radiation of in-service truck tyres. The tyre is modelled as an infinitely long incomplete circular cylindrical shell (see figure 3.9). The effects of inflation pressure and structural damping are included. The normal displacement, velocity and acceleration resulting from a fluctuating load are determined using Flgge's thin shell theory. According to Keltie the amplitude of the waves on the tyre surface decays very rapidly when

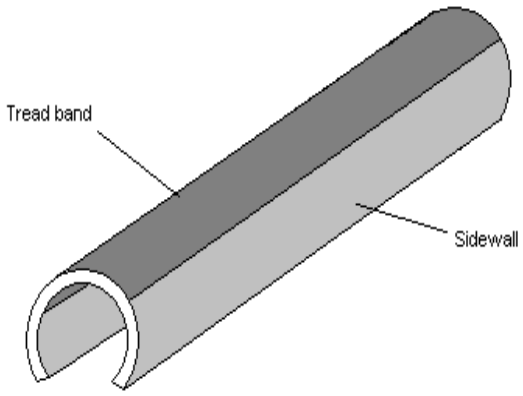

Figure 3.9: Schematic view of the Keltie-model [Keltie, 1982]

moving away from the excitation area. Thus to flexural waves propagating from the contact patch around the periphery, the tyre appears to be of infinite length in the circumferential direction since the waves are damped out before they can see each other near the top of the tyre. Furthermore the tyre material is considered to be isotropic, the shell is considered to be of uniform thickness and the deformations are assumed to be sufficiently small so that they may be considered to be linear elastic deformations. The results of this model are not compared to experiments on real tyres. Therefore it is difficult to say how accurate they are. However, because the tyre is considered to be of infinite length (no curvature) it seems that this model is also not valid below the ring frequency.

3.2.2 Recent usage of shell models

In more recent papers [Kim and Bolton, 2001] and [Kim and Bolton, 2003] shell models are used to investigate the propagation characteristics of the waves that contribute to the tyre's dynamic response. Furthermore they investigate the effects of rotation on the dynamics of a tyre. In [Kim and Bolton, 2001] a FE model is used to model the effect of finite sidewall stiffness and orthotropy resulting from fibre reinforcement of the treadband. This FE model is found to reproduce the major features of tyre dispersion curves: the appearance of tensioned membrane-like flexural wave modes at low frequencies, and the cut on at the tyre's circumferential ring frequency of a fast mode that is primarily associated with extensional motion of the tread band (see figure 3.10).For a schematic view of these modes see figure 2.5. In [Kim and Bolton, 2003] the effects of rotation are examined using a cylindri-

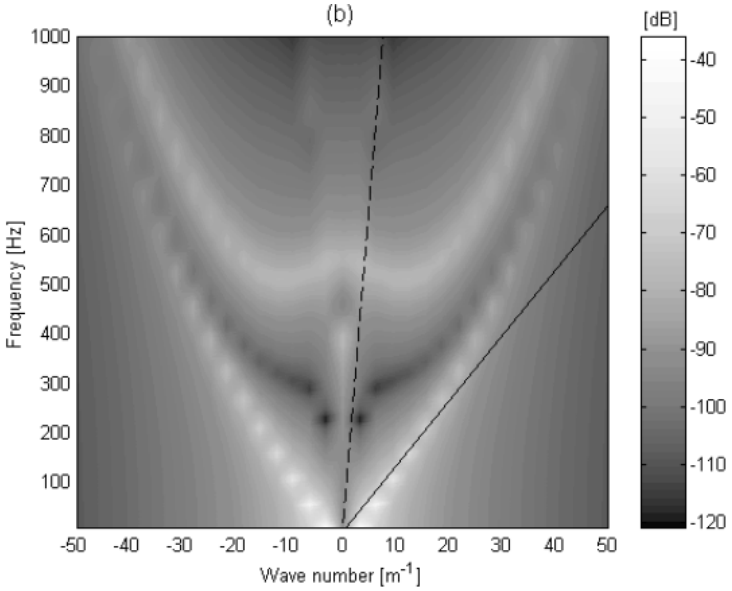

Figure 3.10: Dispersion relations for circular cylindrical shell supported by springs and dampers along the edges of the treadband, dashed line - asymptotic quasi-longitudinal, solid line - equivalent tensioned membrane [Kim and Bolton, 2001]

cal shell model. Based on the results with their model, they conclude that at typical rotation speeds it may be possible to use a stationary tyre analysis to predict the dispersion characteristics of a rotating tyre after a simple kinematic compensation. The effect of rotation on the dispersion characteristics can be seen in figure 3.11 a) and b). Here negative values for k indicate waves running in counterrotating direction ("upstream") and positive values indicate waves running in the same direction as the rotation ("downstream"). The relation for mapping the stationary forced response onto the rotational response is:

$$f = f_s + \frac{k_\phi a}{2\pi}\Omega \tag{3.8}$$

where:

- f_s : stationary tyre natural frequency $[Hz]$
- k_ϕ : wave number $[m^{-1}]$
- Ω : tyre rotational velocity $[rad/s]$

- f : rotation compensated tyre natural frequency $[Hz]$

According to Kim and Bolton this is allowed because the rotational stiffness effect is negligible at normal rotation speeds for car tyres (up to 100 rad/s).

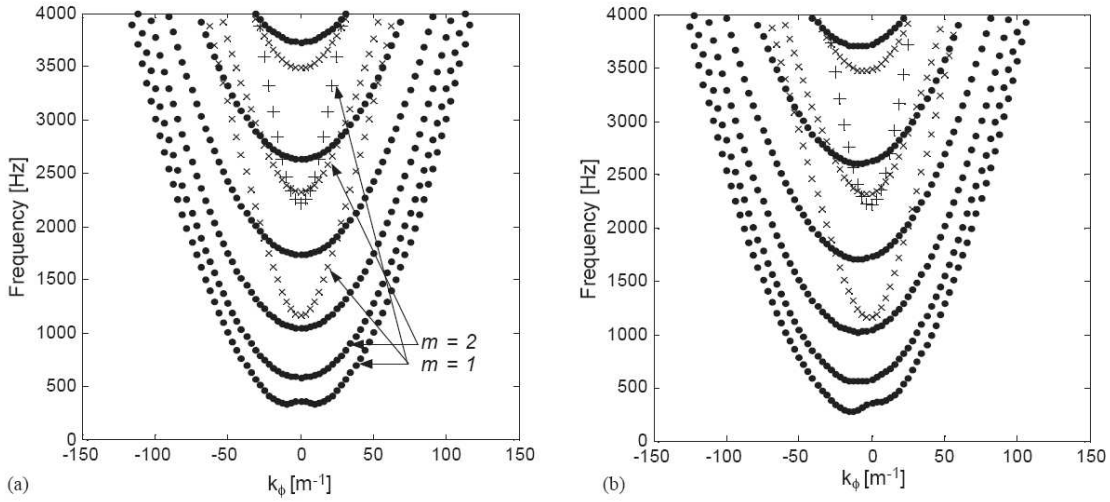

Figure 3.11: Dispersion relations o, flexural wave, x, shear wave, and +, longitudinal (in-plane stretching) wave. (a) Natural frequencies when rotation velocity is 0 (b) natural frequencies in reference coordinates when rotation velocity is 100 rad/s [Kim and Bolton, 2003]

3.2.3 Discussion of shell models

Using analytical shell models has the advantage that it significantly reduces calculation time. The shell models also include the curvature of the tyre, making them valid below the ring frequency. However using analytical shell models has disadvantages also. First it is difficult to incorporate the correct cross-sectional geometry in an analytical model. Secondly, the determination of the correct material properties that have to be used is very difficult because of the different layer in the tyre. Furthermore for certain boundary conditions (e.g. contact) it is very difficult or impossible to find an analytical solution. The use of shell models in FE analysis eliminates the first and last problems. However the problem of how to find the correct material parameters remains.

3.2.4 Semi-analytical models

Because of the axial symmetry of undeformed tyres, it is desirable to exploit this in their modelling and analysis. One way to do this is by using Fourier finite elements. Here the variables and loads around the circumference are represented by a Fourier transform in the circumferential coordinate, while the cross-section is discretised using finite elements. This approach is used in [Noor et al., 1990] for aircraft tyres. However this article does not discuss the vibrational response of the tyre. Neither does it address the contact problem. It simply uses a measured pressure distribution. This excludes an important difficulty: to determine the deformation of the tyre, the forces in the contact patch have to be known, however these are unknown a priori. In [Richards, 1991], the tyre is also modelled using Fourier finite elements. In this article the model is used to investigate the influence of

the cavity resonance on the inertance response and the force transmissibility of the tyre. The model considers small linear perturbations around the inflated axisymmetric state. The inflated state is first determined during a non-linear, static analysis. However the contact problem is not addressed in this paper either. Nilsson and Finnveden [Nilsson and Finnveden, 2002] use an approach which they call waveguide finite elements. A more elaborate discussion of this technique can be found in [Nilsson, 2004]. Here a car tyre is modelled with waveguide finite elements. The model includes the tyre, the wheel and the air cavity enclosed by the tyre-wheel assemblage. Calculations of point mobility and transfer mobilities of a freely suspended tyre/wheel are compared to measurements. The results indicate good agreement in a frequency regions from about 100 Hz up to about 600 Hz. However they also do not treat the contact problem nor do they use different layers, which is possible however. In [Kessels, 2001] the Fourier finite element method is described to model the dynamic behaviour of axisymmetric structures consisting of anisotropic linear elastic/viscoelastic materials. Although this thesis is mainly focussed towards MRI scanners, the method is applicable to other axisymmetric structures also.

3.3 Numerical modelling

When looking for purely numerical models (FEM) used for determining the dynamic response of a tyre up to high frequencies, it is hard to find recent literature on this subject. Either tyre manufacturers carry out all work on this subject in-house, or detailed numerical models are not being used for this purpose because of the large number of elements needed to describe the vibrations at high frequencies accurately. The most recent literature on the dynamic behaviour of tyres using FEM are [Takagi and Takanari, 1991], [Kung, 1990], [Brinkmeier, 2003] and Brinkmeier et al. [2004]. In [Takagi and Takanari, 1991], a tyre is modelled using plane finite elements. To account for the different material layers in the tyre, compound material characteristics are used. The material is assumed to be linear. Tyre pressure, patch deformation and tyre rotation is taken into account. The analysis is carried out in the frequency range 0-250 Hz. Afterwards the results are compared to measurements but there is a large difference. In [Kung, 1990], the tyre is modelled using non-linear laminated shell elements with membrane and bending stiffness. The contact with the road is not taken into account. The modes (0-250 Hz) are determined and compared to measurements. The frequencies at which the natural modes occur are about the same as in the measurements, however the amplitude of the frequency response shows significant deviations from the measurements. In Brinkmeier's thesis [Brinkmeier, 2003] a methodology is described to determine the (complex) eigenvalues of a rolling tyre in ground contact. The stationary rolling contact problem is solved by an Arbitrary Lagrangian Eulerian (ALE) approach (see [Nackenhorst, 2004]). In this approach the rotation of the tyre is accounted for by letting the material flow through the mesh. The deformation of the tyre due to the tyre/road contact is accounted for by a deformation of the (non-rotating) mesh. Subsequently an eigenvalue calculation is performed on the stationary-rolling deformed structure. Gyroscopic effects arise and the eigenvalue-problem becomes a wave theory problem leading to the same eigenvalue shift occurs as described by Kim and Bolton [2003]. Future investigations concerning material damping and nonlinear material behaviour at high frequencies have to be done. Brinkmeier's thesis however only describes the calculation of the eigenvalues, it does not treat the excitation by the road texture.

3.4 Conclusion

From the previous chapters of available analytical models most models have problems describing the vibrational properties of a tyre in the complete frequency range 50-1000 Hz. Ring models can only describe the behaviour up to 300 Hz, because they do not consider displacement variations across the tyre width. The other models (Muggleton, Pinnington and Kropp) that are discussed are only valid above the ring frequency (400 Hz), because they neglect the curvature of the tyre. The only analytical model, which is able to describe the dynamic behaviour in the desired frequency range, is a shell model. But as mentioned earlier, these models have other problems, e.g. the contact problem. Apart from all this all analytical models have another drawback: smeared out material properties have to be used and it is very difficult to determine these properties correctly. Semi-analytical models (e.g. Fourier Finite elements) do not have this problem, because the different layers within the tyre can be modelled separately. These models still have to deal with the contact problem. It is possible to apply an asymmetric load around the circumference that can simulate the contact with the road, however the forces generated by the road contact are unknown a priori. So some kind of contact model has to be connected to the Fourier FE analysis and a very large number of harmonics may be necessary to describe the deformation. It seems that fully detailed numerical models are not used much to perform frequency analysis. This probably has to do with the large number of elements needed to describe the vibrations at high frequencies accurately. However the approach used by Brinkmeier [Brinkmeier, 2003] seems to be a relatively easy way to incorporate all of the material and geometrical properties into the model without excessive calculation times.

Summarizing, all analytical models have smeared out material properties, which are difficult to determine. For the semi-analytical approaches it is difficult to describe the contact with the road. Therefore determining the eigenvalues and eigenmodes of a detailed FE-model of the tyre and then using these to construct a modal base of the tyre seems a computationally cheap way of calculating the time-domain response of the tyre. This approach is thus further examined in this thesis.

Chapter 4

Tyre behaviour

As mentioned in the previous chapter constructing a modal base of the tyre in the stationary rolling situation could be a computationally cheap way of calculating the time domain response of a car tyre. However before this is done some other analysis is performed to get a better insight into the dynamic behaviour of tyres. In this preliminary analysis the influence of the tyre/road contact and rotation on the dynamics of the tyre are investigated.

4.1 The FE model

In this chapter some properties of a tyre are examined using a FE model of a tyre. As we are only interested in the qualitative behaviour of the tyre at this point the example model of a 175SR14 tyre from ABAQUS is used. This (relatively simple) model is believed to include the basic properties of a car tyre and is described in the next section. The cross-section of the tyre is modelled as shown in figure 4.1. The tread and sidewalls are made of rubber, and the belts and carcass are constructed from

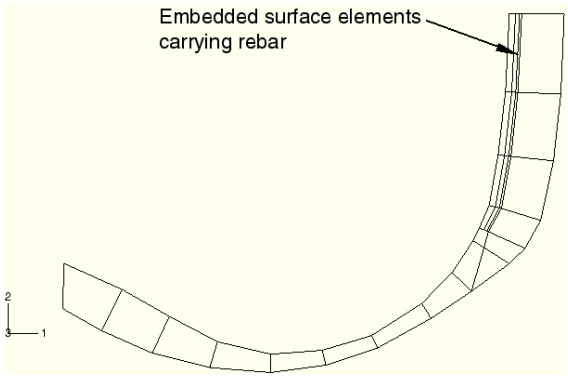

Figure 4.1: FE model of one half of the tyre cross section.

fiber-reinforced rubber composites. The rubber is modelled as an incompressible hyper/visco-elastic material, and the fiber reinforcement is modelled as a linear elastic material. This reinforcement is modelled by using embedded surface elements carrying rebar. This rebar option is used to define layers of uniaxial reinforcement in membrane, shell, and surface elements. This cross-section is rotated about an axis to generate the 3D tyre model. To see whether the results from this model are realistic a static analysis is performed with this model. The quantitative results are not important here, we are only concerned with the qualitative behaviour, which should look like results from literature.

The results from the static analysis can be seen in figure 4.2. In this analysis the tyre is pressed against a rigid surface (the road) and the displacement and forces are determined. When this result

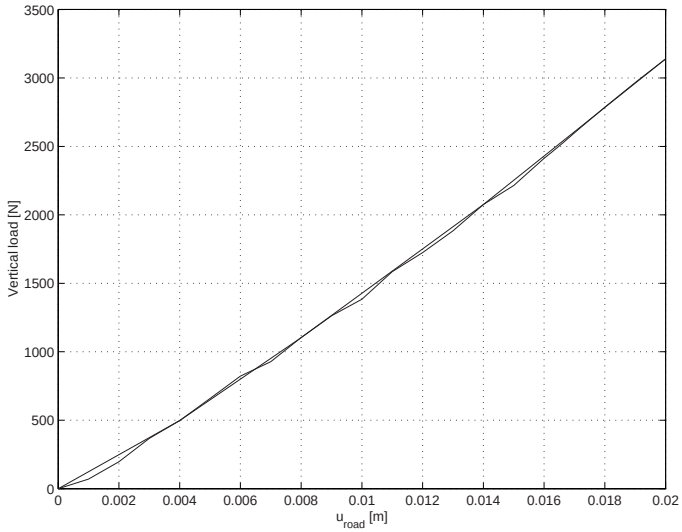

Figure 4.2: Force-displacement of the FE model . The hub is fixed and the road is moved.

is compared to the results from figure 4.3 it can be seen that the two resemble each other well. They both show a linear behaviour and even the magnitudes of the force and displacement are about the same. The results from [Burke and Olatunsbosun, 1997] show a slightly stiffer tyre, but differences are expected as the Abaqus model is very simple and the dimensions of the tyre are different. Taking this into account it is a remarkable coincidence that the results from the Abaqus model compare so well to the results from [Burke and Olatunsbosun, 1997]. However the qualitative behaviour of the Abaqus model, which is the main reason for this comparison, is good.

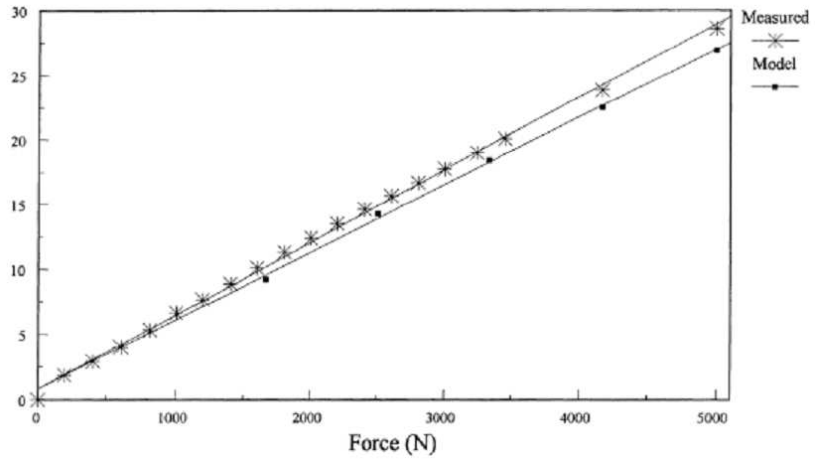

Figure 4.3: Force-displacement results for a 195/65R15 car tyre. The vertical axis shows the displacement in mm. See [Burke and Olatunsbosun, 1997]

4.2 Analysis

4.2.1 Contact

First of all the influence of the tyre/road contact on the dynamic behaviour of the tyre is investigated. If the deformation of the tyre due to the static load has no influence on the dynamic behaviour of the tyre, this deformation may be neglected. This would greatly simplify the analysis as the tyre then remains axisymmetric. To investigate this, the tyre is pressed against the road surface with different static forces F(0 N, 300 N, 2000 N, 3300 N and 4500 N). After equilibrium is reached a dynamic force dF(200 N) is added to this static load and a steady-state frequency response analysis is performed.(see figure 4.4). The results for this analysis around the first mode can be seen in figure 4.5

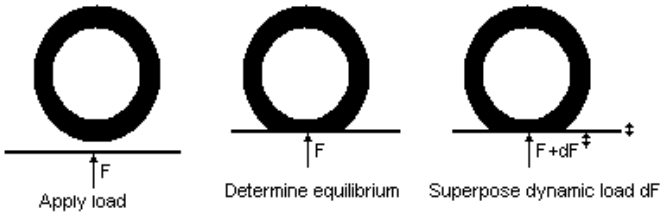

Figure 4.4: Schematic view of the analysis.

(solid lines). In this figure it seems that the eigenfrequency decreases as the static load increases. This is in contradiction with what one might expect to happen. As a preload normally increases stiffness one would expect that the eigenfrequency increases with increasing preload, just as increasing the tension in a guitar increases the tone. During the static analysis the points which are in contact with

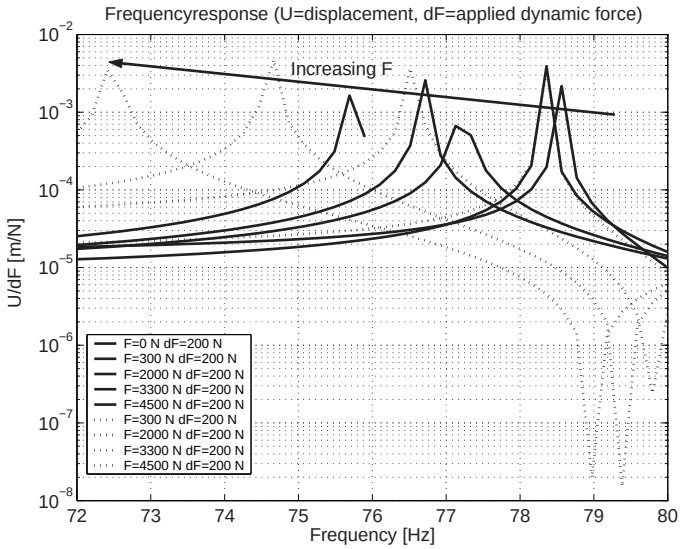

Figure 4.5: FRF's of the Abaqus example tyre. dF on road: solid lines. dF on single node: dashed lines.

the road are determined and all these points stay closed (stay connected to the road) in the steady

state analysis. Therefore these points cannot move relative to each other. To check the influence of this constraint on the response another approach is used. First the contact pressure at each node is determined during a static contact analysis. Then, in a new analysis, this force distribution is applied to the ”contact” nodes and a static analysis is performed. After this a steady-state dynamic analysis is carried out with the dynamic load applied to the centre-node of the contact patch. The results from this analysis are also shown in figure 4.4 (dashed lines). The shift of the frequencies still occurs. The fact that the resonance frequencies are lower in this case is caused by the relaxation of the problem (the nodes in the contact patch are no longer constrained). There are two possible reasons for the fact that the resonance frequencies for preloaded tyres are lower than the resonance frequency of a unloaded tyre (F=0). The first one lies in the geometric deformation of the tyre due to the load. The tyre looses its curvature in the contact patch which might cause a decrease in the local stiffness. The second possible reason lies in the fact that the tension in the treadbelt decreases as the tyre is loaded. This might cause the eigenfrequency to decrease. This is the same effect as when the tension in a guitar string is increased, which is rea To test this, two analyses are done:

- Undeformed tyre and a point load on node 18055 (the centre-node of the contact patch in case of contact)
- Load distribution for a static load of 4500 N and a point load on node 18055. This static load is determined in a preceding contact analysis where the tyre is pressed against the road with 4500N.

The results for this analysis are shown in figure 4.6. The local stiffness for the preloaded case is

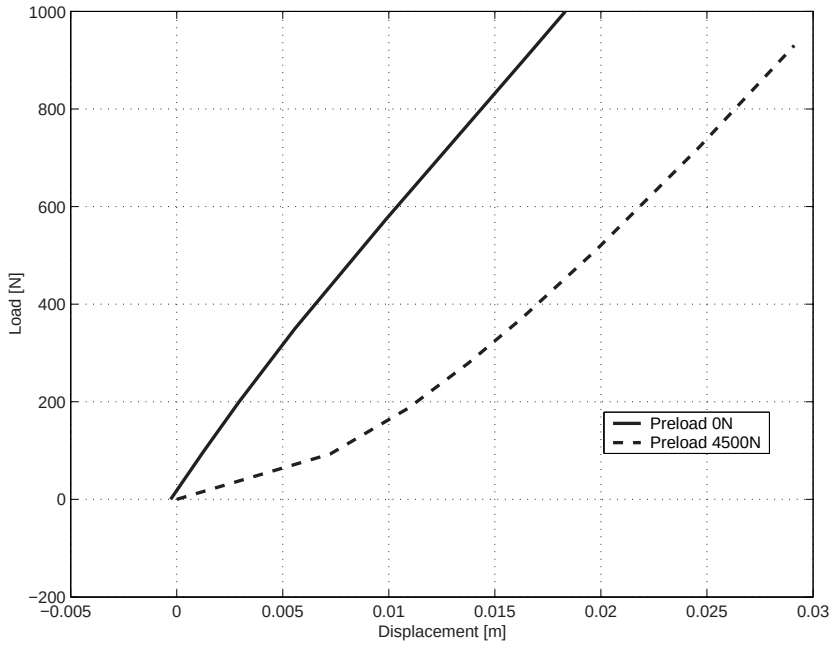

Figure 4.6: Force displacement of the centerpoint of the contact patch (node 18055) with and without preload.

indeed lower, this however does not point out which of the two effects is most important. However if one looks at the tension in the belt of a loaded and an unloaded tyre, figure 4.7 and 4.8, it can be seen from these figures that loading the tyre has a significant effect on the stress in the tyre belt (from tension to compression!). This suggests that this effect is probably the cause of the shift of

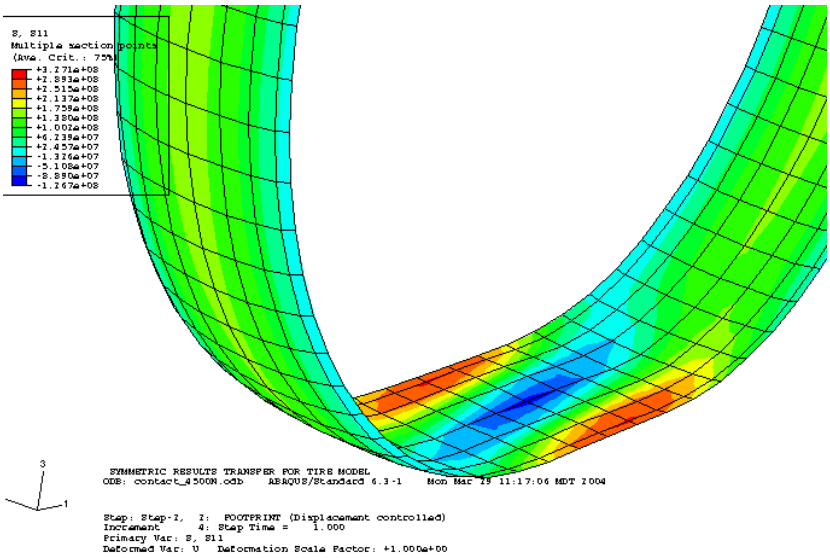

Figure 4.7: Stress in belt layer 1, when the tyre is loaded with 4500N . Legend: Max Stress (Red) = 327.1MPa, Min Stress (Blue) = -126.7 MPa

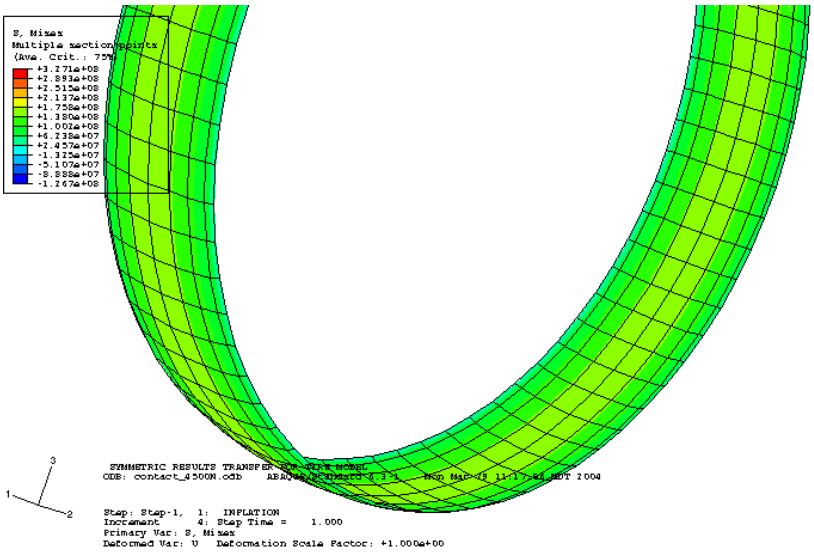

Figure 4.8: Stress in belt layer 1, when the tyre is not loaded (only inflated). Legend: Max Stress (Red) = 327.1MPa, Min Stress (Blue) = -126.7 MPa.

the resonance frequencies. The main result of these simulations is that the static load acting on the tyre has a significant influence on the dynamic behaviour of the tyre and for this reason the local deformation and the related stress distribution have to be taken into account. A lot of models, e.g.

the Chalmers model, do not take this into account. Probably because it may not be very important at higher frequencies and as the Chalmers model is only valid above 400 Hz anyway this may not be a problem. However if one wants to be able to predict tyre-vibrations at lower frequencies too, the effect of the tyre/road contact has to be taken into account. When using a modal approach this is relatively easy. One can then simply determine the modes and eigenvalues in the deformed situation.

4.2.2 Rotation

Another very important factor which has to be taken into account is the rotation of the tyre. As mentioned in section 3.2.2 this has an important influence on the slope of the dispersion curves. In figure 4.9 the dispersion curves of the Abaqus example tyre are shown. The points shown in the figure show the shift of the dispersion curves at 40, 80 and 120 km/h according to (3.8). Again negative values for k indicate waves running in counterrotating direction (”upstream”) and positive values indicate waves running in the same direction as the rotation (”downstream”). Clearly the rotation has a significant influence on the dynamic behaviour of the tyre and therefore has to be considered. This can be seen as a Doppler effect. Waves running upstream are compressed, while waves running downstream are stretched. Taking this effect into account is not as straightforward as taking the influence of the tyre/road contact into account. In the next chapter this problem is discussed.

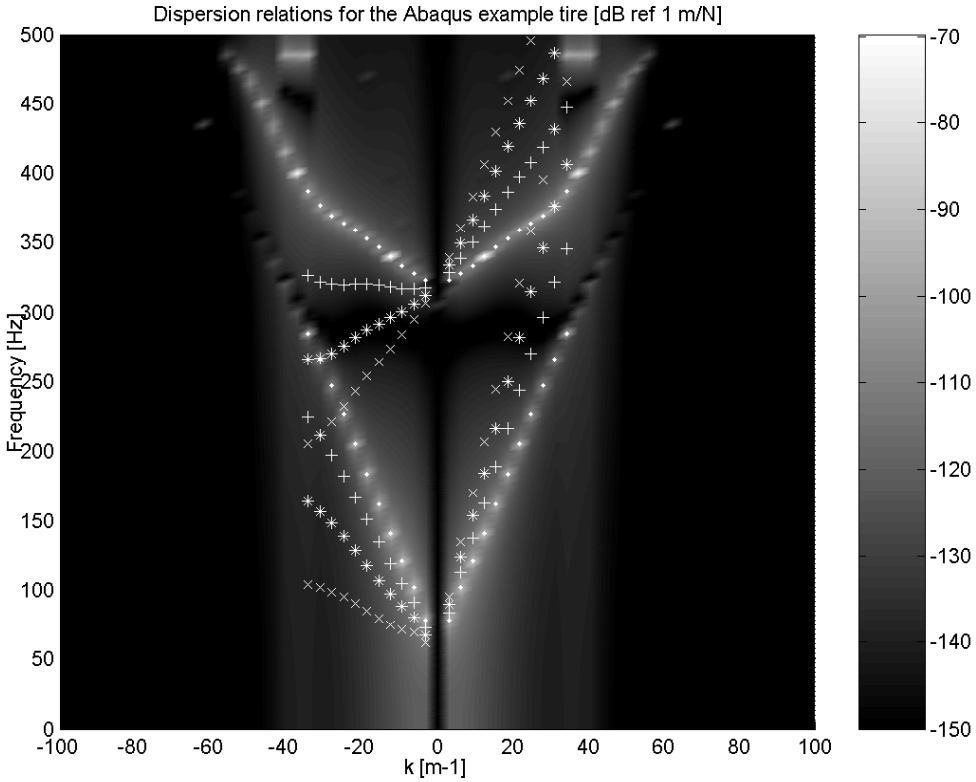

Figure 4.9: Dispersion relations for the Abaqus example tire •: 0 km/h, +: 40 km/h,∗: 80 km/h and ×: 120 km/h

Chapter 5

Theory

As concluded in chapter 3 using a modal approach to calculate the time domain response of a tyre may be a computationally cheap approach. The large and nonlinear deformation of the tyre is determined using the full system of equations. Subsequently the modal base is constructed around this state, thus taking the effect of the tyre/road contact into account. The response of the tyre due to the road unevenness may then be determined using the modal superposition principle. However the effect of the rotation of the tyre also has to be taken into account. In [Brinkmeier, 2003] this is done by using an ALE-approach (see [Nackenhorst, 2004]) which leads to the following linearized (undamped) finite element equations for small amplitude vibrations:

$$\mathbf{M}\ddot{\mathbf{u}}(t) + \mathbf{G}\dot{\mathbf{u}}(t) + (\mathbf{K} - \mathbf{W})\mathbf{u}(t) = \mathbf{f}(t) \tag{5.1}$$

where $\mathbf{M}$ is the mass matrix, $\mathbf{G}$ is the skew-symmetric gyroscopic matrix, $\mathbf{K}$ is the stiffness matrix and $\mathbf{W}$ is a symmetric matrix resulting from the linearization of the inertia forces due to stationary rolling. $\mathbf{u}$ represents the small displacements of transient motion which are measured relatively to the large deformations caused from stationary rolling. $\mathbf{f}(t)$ describes the transient excitation forces. This leads to the following quadratic eigenvalue problem.

$$[\lambda^2\mathbf{M} + \lambda\mathbf{G} + (\mathbf{K} - \mathbf{W})]\mathbf{z} = 0 \tag{5.2}$$

where λ are the complex eigenvalues and $\mathbf{z}$ the complex eigenvectors. This is transformed into a linear eigenvalue problem with the substitution $\hat{\mathbf{z}}^T = [\lambda\mathbf{z}, \mathbf{z}]$:

$$\left[\begin{pmatrix} -\mathbf{G} & -(\mathbf{K} - \mathbf{W}) \\ \mathbf{I} & \mathbf{0} \end{pmatrix} - \lambda \begin{pmatrix} \mathbf{M} & \mathbf{0} \\ \mathbf{0} & \mathbf{I} \end{pmatrix}\right] \hat{\mathbf{z}} = \mathbf{0} \tag{5.3}$$

Once the eigenvalues from (5.3) have been determined, the transient response can be determined using the modal superposition principle. The commercially available FE packages are capable of performing a steady state rolling simulation. However at the moment it is not possible to perform an eigenvalue analysis in the stationary rolling situation. The $\mathbf{G}$ matrix is not considered for this situation, which means the splitting of the eigenvalues does not occur. Therefore another way has to be found to incorporate the effect of rotation. This approach and its implementation are described in the following sections. Also the contact model used for this analysis is described. The derivation in the following sections applies to the 2D situation of a ring. However the derivation for the 3D case is exactly the same.

5.1 Definitions

First of all a little note on the notation used in this chapter. Matrices are denoted in bold (e.g. the mass matrix **M**), while vectors can be recognized by the $\vec{}$ above the variable.
In this chapter two coordinate systems are used: $\vec{\mathbf{e}}^1$ and $\vec{\mathbf{e}}^2$. $\vec{\mathbf{e}}^1$ is the reference coordinate system that is fixed to the center of the tyre and translates together with the tyre, but does not rotate. $\vec{\mathbf{e}}^2$ is a body-fixed coordinate system. This means that this system rotates along with the ring at velocity Ω. See figure 5.1. In these systems the angles α (in the body-fixed frame) and β in the reference frame are defined, so that for a certain point k on the ring $\beta_k = \alpha_k + \Omega t$. The rotation matrix $\mathbf{A}^{21}(t)$ so that

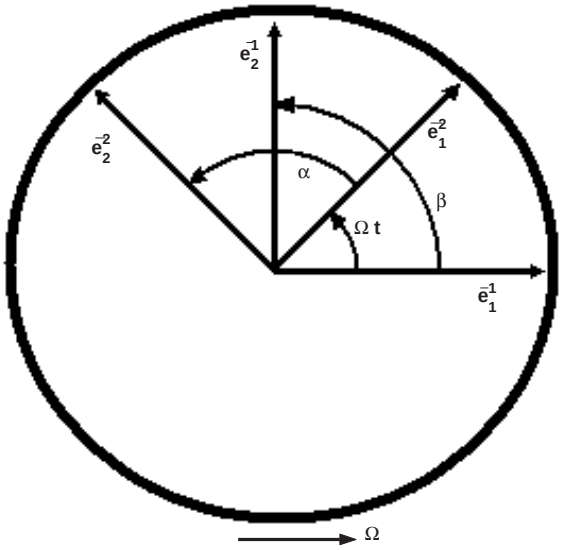

Figure 5.1: The coordinate systems.

$\vec{\mathbf{e}}^2 = \mathbf{A}^{21}\vec{\mathbf{e}}^1$ is:

$$\mathbf{A}^{21}(t) = \begin{pmatrix} \cos(\Omega t) & \sin(\Omega t) \\ -\sin(\Omega t) & \cos(\Omega t) \end{pmatrix} \tag{5.4}$$

where Ω is the rotational velocity of the rotating reference frame. The derivative of the rotation matrix is:

$$\dot{\mathbf{A}}^{21}(t) = \begin{pmatrix} -\Omega\sin(\Omega t) & \Omega\cos(\Omega t) \\ -\Omega\cos(\Omega t) & -\Omega\sin(\Omega t) \end{pmatrix} = \begin{pmatrix} 0 & \Omega \\ -\Omega & 0 \end{pmatrix} \mathbf{A}^{21}(t) = \hat{\mathbf{\Omega}}\mathbf{A}^{21}(t) \tag{5.5}$$

where

$$\hat{\mathbf{\Omega}} = \begin{pmatrix} 0 & \Omega \\ -\Omega & 0 \end{pmatrix} \tag{5.6}$$

And the second derivative is:

$$\ddot{\mathbf{A}}^{21}(t) = \begin{pmatrix} -\Omega^2 & 0 \\ 0 & -\Omega^2 \end{pmatrix} \mathbf{A}^{21}(t) = \hat{\mathbf{\Omega}}^2\mathbf{A}^{21}(t) \tag{5.7}$$

For the time being, the excitation is defined as a point force that acts at a fixed position in the reference frame. In the reference frame $\vec{\mathbf{e}}^1$ this force can thus be written as:

$$\mathbf{F}^{1T}\vec{\mathbf{e}}^1 = \begin{pmatrix} F_x\delta(\beta) \\ F_y\delta(\beta) \end{pmatrix}^T \vec{\mathbf{e}}^1 \tag{5.8}$$

with

$$\mathbf{F}^1 = \begin{pmatrix} F_x\delta(\beta) \\ F_y\delta(\beta) \end{pmatrix} \tag{5.9}$$

This leads to a ”rotating” force in the body fixed system:

$$\mathbf{F}^{2T}\vec{\mathbf{e}}^2 = \begin{pmatrix} F_x\delta(\alpha+\Omega t) \\ F_y\delta(\alpha+\Omega t) \end{pmatrix}^T \mathbf{A}^{12}\vec{\mathbf{e}}^2 \tag{5.10}$$

where

$$\mathbf{A}^{12} = (\mathbf{A}^{21})^{-1} = (\mathbf{A}^{21})^T \tag{5.11}$$

and

$$\mathbf{F}^2 = \mathbf{A}^{21}\begin{pmatrix} F_x\delta(\alpha+\Omega t) \\ F_y\delta(\alpha+\Omega t) \end{pmatrix} \tag{5.12}$$

5.2 Rotating modes

As has been pointed out in the previous chapter the tyre/road contact has a significant influence on the tyre dynamics. Seen from a modal point of view it leads to the modes being non-axisymmetric. In the undeformed state a tyre has rotation symmetric modes. At each eigenvalue there are two modeshapes which are the same, only rotated $\frac{180}{2n}$ degrees, where n is the number of waves along the circumference, see e.g. figure 5.2. This means that at a location where one mode has a maximum displacement, the

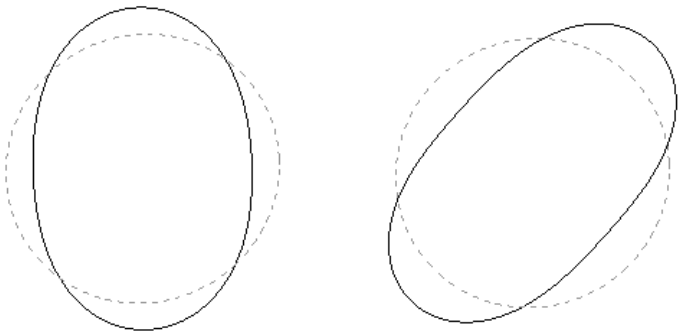

Figure 5.2: Example of two degenerated modes with $n = 2$.

other mode has zero displacement. When the tyre is excited by a point force two modes of the same frequency always combine in such a way that the maximum displacement is always in the direction of the excitation force. However, when the tyre is in contact with the ground this is not the case anymore. The modes are already oriented due to the initial deformation. Also they are not rotation symmetric anymore. If we now want to calculate the response of the tyre in the local coordinate system by rotating a force or constraint (the road) around the tyre, the modes (and thus also the mass and stiffness matrices) have to rotate along with this excitation. This means that there are two situations:

1) The modes (and **K** and **M** matrices) are fixed to the rotating frame $\vec{\mathbf{e}}^2$. A certain mode $\vec{\phi}_{bf}$ which is fixed to the body fixed frame (indicated by the subscript bf) can thus be described as follows:

$$\vec{\phi}_{bf} = \boldsymbol{\phi}_{bf}^{2T}\vec{\mathbf{e}}^2 = \begin{pmatrix} \phi_x(\alpha) \\ \phi_y(\alpha) \end{pmatrix}^T \vec{\mathbf{e}}^2 = \begin{pmatrix} \phi_x(\beta - \Omega t) \\ \phi_y(\beta - \Omega t) \end{pmatrix}^T \mathbf{A}^{21}\vec{\mathbf{e}}^1 \tag{5.13}$$

This means that a mode which is constant in the body fixed frame is time-dependent in the reference frame. Matrix $\boldsymbol{\Phi}_{bf}^2$ (the body fixed modes in frame $\vec{\mathbf{e}}^2$) containing m modes can now be defined as:

$$\boldsymbol{\Phi}_{bf}^2 = \begin{pmatrix} \boldsymbol{\phi}_{bf,1}^2 & \dots & \boldsymbol{\phi}_{bf,m}^2 \end{pmatrix} \tag{5.14}$$

where

$$\boldsymbol{\phi}_{bf,m}^2 = \begin{pmatrix} \phi_{mx}(\alpha) \\ \phi_{my}(\alpha) \end{pmatrix} \tag{5.15}$$

For the mass matrix this means:

$$\mathbf{M}_{bf}^2(\alpha) = \mathbf{A}^{21}(\Omega t)\mathbf{M}_{bf}^1(\beta - \Omega t)\mathbf{A}^{12}(\Omega t) \tag{5.16}$$

The same is valid for stiffness matrix.
2) The modes (and **K** and **M** matrices) are fixed to the reference frame $\vec{\mathbf{e}}^1$, which means that they rotate along with the excitation in the body fixed frame. A mode $\vec{\phi}_{rf}$ which is fixed to the reference frame can be described as follows:

$$\vec{\phi}_{rf} = \boldsymbol{\phi}_{rf}^{1T}\vec{\mathbf{e}}^1 = \begin{pmatrix} \phi_x(\beta) \\ \phi_y(\beta) \end{pmatrix}^T \vec{\mathbf{e}}^1 = \begin{pmatrix} \phi_x(\alpha + \Omega t) \\ \phi_y(\alpha + \Omega t) \end{pmatrix}^T \mathbf{A}^{12}\vec{\mathbf{e}}^2 \tag{5.17}$$

This means that a mode which is constant in the reference frame is time-dependent in the body-fixed frame. Matrices $\boldsymbol{\Phi}_{rf}^i$ containing m modes can now be defined as:

$$\boldsymbol{\Phi}_{rf}^i = \begin{pmatrix} \boldsymbol{\phi}_{rf,1}^i & \dots & \boldsymbol{\phi}_{rf,m}^i \end{pmatrix} \text{ with } i = 1, 2 \tag{5.18}$$

where

$$\boldsymbol{\phi}_{rf,m}^1 = \begin{pmatrix} \phi_{mx}(\beta) \\ \phi_{my}(\beta) \end{pmatrix} \tag{5.19}$$

and

$$\boldsymbol{\phi}_{rf,m}^2 = \mathbf{A}^{21}\begin{pmatrix} \phi_{mx}(\alpha + \Omega t) \\ \phi_{my}(\alpha + \Omega t) \end{pmatrix} \tag{5.20}$$

For the mass matrix this means:

$$\mathbf{M}_{rf}^1(\beta) = \mathbf{A}^{12}(\Omega t)\mathbf{M}_{rf}^2(\alpha + \Omega t)\mathbf{A}^{21}(\Omega t) \tag{5.21}$$

Again the same is valid for stiffness matrix. In the next 2 sections both cases, body fixed modes and reference frame fixed modes, are described for the body fixed frame $\vec{\mathbf{e}}^2$.

5.3 Body fixed modes

After Abaqus has assembled the mass (**M**) and stiffness (**K**) matrices the following set of equations describes the (undamped) system (5.22). For the body fixed modes $\mathbf{M}^2_{bf}(\alpha) = \mathbf{M}$ and $\mathbf{K}^2_{bf}(\alpha) = \mathbf{K}$ so:

$$\mathbf{M}\ddot{\mathbf{u}}^2(t) + \mathbf{K}\mathbf{u}^2(t) = \mathbf{F}^2(t) \tag{5.22}$$

where $\mathbf{u}^2(t)$ is the displacement colunm and $\mathbf{F}^2(t)$ is the load column in $\vec{\mathbf{e}}^2$.

$$det(\mathbf{K} - \omega_n^2\mathbf{M}) = 0 \tag{5.23}$$

(5.22) can be uncoupled using the eigenvectors and eigenvalues of the above system (5.23).We now take:

$$\mathbf{u}^2(t) = \mathbf{\Phi}^2_{bf}\boldsymbol{\eta}(t) \tag{5.24}$$

where $\mathbf{\Phi}$ is a $ndof * nom$ (where $ndof$ is the number of degrees of freedom (DOF) and nom is the number of used eigenmodes) matrix containing the mass-normalized eigenvectors and $\boldsymbol{\eta}(t)$ is the vector containing the modal coordinates. This means that

$$\mathbf{\Phi}^{2T}_{bf}\mathbf{M}\mathbf{\Phi}^2_{bf} = \mathbf{I} \tag{5.25}$$

and

$$\mathbf{\Phi}^{2T}_{bf}\mathbf{K}\mathbf{\Phi}^2_{bf} = \mathbf{V} \tag{5.26}$$

where **V** is a diagonal matrix containing the eigenvalues. We can now substitute (5.24) into (5.22) and pre-multiply by $\mathbf{\Phi}^T$, which leads to:

$$I\ddot{\boldsymbol{\eta}}(t) + \mathbf{V}\boldsymbol{\eta}(t) = \mathbf{\Phi}^{2T}_{bf}\mathbf{F}^2(t) \tag{5.27}$$

Including damping can be done by adding $\mathbf{D}_{mod}\dot{\boldsymbol{\eta}}(t)$ to the left-hand-side of (5.27). Where $\mathbf{D}_{mod}$ is a diagonal matrix containing modal damping terms d_{kk} defined by:

$$d_{kk} = 2\zeta_k\omega_k \tag{5.28}$$

If all eigenmodes are used ($nom = ndof$) the number of equations is not reduced, it simply is a coordinate transformation then. However if the number of eigenmodes that is used is less ($nom < ndof$) the number of equations is reduced to the number of modes. All these equations are uncoupled and look like this:

$$\ddot{\boldsymbol{\eta}}(t)_k + 2\zeta_k\omega_k\dot{\boldsymbol{\eta}}(t)_k + \omega_k^2\boldsymbol{\eta}(t)_k = \mathbf{\Phi}^{2T}_{bf,k}\mathbf{F}^2(t) \tag{5.29}$$

Or in matrix notation:

$$\ddot{\boldsymbol{\eta}}(t) + \mathbf{D}_{mod}\dot{\boldsymbol{\eta}}(t) + \mathbf{V}\boldsymbol{\eta}(t) = \mathbf{\Phi}^{2T}_{bf}\mathbf{F}^2(t) \tag{5.30}$$

Also Rayleigh damping may be used:

$$\mathbf{D} = \gamma_1\mathbf{M} + \gamma_2\mathbf{K} \tag{5.31}$$

Leading to a slightly modified equation:

$$\ddot{\boldsymbol{\eta}}(t)_k + (\gamma_1 + \gamma_2\omega_k^2)\dot{\boldsymbol{\eta}}(t)_k + \omega_k^2\boldsymbol{\eta}(t)_k = \mathbf{\Phi}^{2T}_{bf,k}\mathbf{F}^2(t) \tag{5.32}$$

And again in matrix notation:

$$\ddot{\boldsymbol{\eta}}(t) + (\gamma_1\mathbf{I} + \gamma_2\mathbf{V})\dot{\boldsymbol{\eta}}(t) + \mathbf{V}\boldsymbol{\eta}(t) = \mathbf{\Phi}^{2T}_{bf}\mathbf{F}^2(t) \tag{5.33}$$

It is relatively simple to solve these equations. The set of second order differential equations is transformed into a set of first order differential (see (5.3) for the undamped case) equations which can be solved by using for example ode45 in Matlab.

$$\dot{\mathbf{y}} = \begin{bmatrix} \mathbf{0} & \mathbf{I} \\ -\mathbf{V} & \mathbf{0} \end{bmatrix} \begin{bmatrix} \boldsymbol{\eta}(t) \\ \dot{\boldsymbol{\eta}}(t) \end{bmatrix} + \begin{bmatrix} \mathbf{0} \\ \boldsymbol{\Phi}_{bf}^{2T} \mathbf{F}^2(t) \end{bmatrix} \tag{5.34}$$

where

$$\mathbf{y} = \begin{bmatrix} \boldsymbol{\eta}(t) \\ \dot{\boldsymbol{\eta}}(t) \end{bmatrix} \tag{5.35}$$

When $\boldsymbol{\eta}(t)$ is known the real displacements $\boldsymbol{u}$ can be determined by pre-multiplying $\boldsymbol{\eta}$ by $\boldsymbol{\Phi}_{bf}^2$.

5.4 Reference frame fixed modes

When using reference frame fixed modes, things get a bit more complicated. Now $\mathbf{M}_{rf}^1(\beta) = \mathbf{M}$ and $\mathbf{K}_{rf}^1(\beta) = \mathbf{K}$. $\mathbf{M}_{rf}^2$ and $\mathbf{K}_{rf}^2$ can be determined with (5.21). $\boldsymbol{\Phi}_{rf}^2(t)$ is not a constant and this has a significant influence on the modal equations. First of all the chain rule has to be applied when differentiating with respect to t.

$$\mathbf{u}^2(t) = \boldsymbol{\Phi}_{rf}^2(t)\boldsymbol{\eta}(t) \tag{5.36}$$

$$\dot{\mathbf{u}}^2(t) = \dot{\boldsymbol{\Phi}}_{rf}^2(t)\boldsymbol{\eta}(t) + \boldsymbol{\Phi}_{rf}^2(t)\dot{\boldsymbol{\eta}}(t) \tag{5.37}$$

$$\ddot{\mathbf{u}}^2(t) = \ddot{\boldsymbol{\Phi}}_{rf}^2(t)\boldsymbol{\eta}(t) + 2\dot{\boldsymbol{\Phi}}_{rf}^2(t)\dot{\boldsymbol{\eta}}(t) + \boldsymbol{\Phi}_{rf}^2(t)\ddot{\boldsymbol{\eta}}(t) \tag{5.38}$$

Substituting (5.36) to (5.38) in (5.22) leads to:

$$I\ddot{\boldsymbol{\eta}}(t) + [2\boldsymbol{\Phi}_{rf}^2(t)^T \mathbf{M}_{rf}^2 \dot{\boldsymbol{\Phi}}_{rf}^2(t)]\dot{\boldsymbol{\eta}} + [\boldsymbol{\Phi}_{rf}^2(t)^T \mathbf{M}_{rf}^2 \ddot{\boldsymbol{\Phi}}_{rf}^2(t) + \mathbf{V}]\boldsymbol{\eta}(t) = \boldsymbol{\Phi}_{rf}^2(t)^T \mathbf{F}^2(t) \tag{5.39}$$

Including a damping matrix $\mathbf{D}$ leads to:

$$\begin{aligned} &I\ddot{\boldsymbol{\eta}}(t) + [2\boldsymbol{\Phi}_{rf}^2(t)^T \mathbf{M}_{rf}^2 \dot{\boldsymbol{\Phi}}_{rf}^2(t) + \boldsymbol{\Phi}_{rf}^2(t)^T \mathbf{D}_{rf}^2 \boldsymbol{\Phi}_{rf}^2(t)]\dot{\boldsymbol{\eta}} + \\ &[\boldsymbol{\Phi}_{rf}^2(t)^T \mathbf{M}_{rf}^2 \ddot{\boldsymbol{\Phi}}_{rf}^2(t) + \boldsymbol{\Phi}_{rf}^2(t)^T \mathbf{D}_{rf}^2 \dot{\boldsymbol{\Phi}}_{rf}^2(t) + \mathbf{V}]\boldsymbol{\eta}(t) = \boldsymbol{\Phi}_{rf}^2(t)^T \mathbf{F}^2(t) \end{aligned} \tag{5.40}$$

It is clear $\dot{\boldsymbol{\Phi}}_{rf}^2(t)$ and $\ddot{\boldsymbol{\Phi}}_{rf}^2(t)$ have to be determined. This significantly increases the computational cost of the problem as those matrices as well as $\boldsymbol{\Phi}_{rf}^2(t)$ have to be calculated at every time step and because the FE model is a discrete model an interpolation proces is needed also. But the main problem here is that the response is calculated in the local coordinate system, which makes it necessary to perform yet another transformation if one wants to calculate the sound radiation from this response. These problems can be avoided by not using Lagrangian coordinates as described above, but using an Eulerian approach, which is described in the next section.

5.5 Eulerian coordinates

The equations of motion of the ring or tyre in the body fixed, lagrangian coordinates are given in (5.22). These equations can be transformed into the reference coordinate system by using the material derivative:

$$\frac{D}{Dt} = \frac{\partial}{\partial t} + \Omega \frac{\partial}{\partial \beta} \tag{5.41}$$

where the left hand side represents the time derivative in the body fixed (Lagrangian) coordinates, the first term on the right hand side is the time derivative in the reference (Eulerian) coordinates, Ω is the rotational speed and β is the circumferential angle in the reference frame. After applying (5.41) the equations can be expressed as:

$$\begin{aligned}
&\mathbf{M}^2_{rf}\frac{D^2\mathbf{u}^2(\alpha+\Omega t,t)}{Dt^2}+\mathbf{K}^2_{rf}\mathbf{u}^2(\alpha+\Omega t,t)=\mathbf{F}^2(t)\\
&\mathbf{M}^2_{rf}\left(\frac{\partial^2\mathbf{u}^2(\alpha+\Omega t,t)}{\partial t^2}+2\Omega\frac{\partial^2\mathbf{u}^2(\alpha+\Omega t,t)}{\partial t\partial\beta}+\Omega^2\frac{\partial^2\mathbf{u}^2(\alpha+\Omega t,t)}{\partial\beta^2}\right)+\mathbf{K}^2_{rf}\mathbf{u}^2(\alpha+\Omega t,t)=\mathbf{F}^2(t)
\end{aligned} \tag{5.42}$$

Now $\mathbf{u}^2(\alpha+\Omega t,t)$ can be rewritten as:

$$\mathbf{u}^2(\alpha+\Omega t,t)=\mathbf{\Phi}^2_{rf}(\alpha+\Omega t,t)\boldsymbol{\eta}(t)=\mathbf{A}^{21}(t)\mathbf{\Phi}^1_{rf}(\beta)\boldsymbol{\eta}(t)=\mathbf{u}^2(\beta,t) \tag{5.43}$$

This leads to the following when substituted in (5.42):

$$\frac{\partial^2\mathbf{u}^2(\beta,t)}{\partial t^2}=\hat{\mathbf{\Omega}}^2\mathbf{A}^{21}\mathbf{\Phi}^1_{rf}(\beta)\boldsymbol{\eta}(t)+2\hat{\mathbf{\Omega}}\mathbf{A}^{21}\mathbf{\Phi}^1_{rf}(\beta)\dot{\boldsymbol{\eta}}(t)+\mathbf{A}^{21}\mathbf{\Phi}^1_{rf}(\beta)\ddot{\boldsymbol{\eta}}(t) \tag{5.44}$$

$$2\Omega\frac{\partial^2\mathbf{u}^2(\beta,t)}{\partial t\partial\beta}=2\Omega\hat{\mathbf{\Omega}}\mathbf{A}^{21}\frac{\partial\mathbf{\Phi}^1_{rf}(\beta)}{\partial\beta}\boldsymbol{\eta}(t)+2\Omega\mathbf{A}^{21}\frac{\partial\mathbf{\Phi}^1_{rf}(\beta)}{\partial\beta}\dot{\boldsymbol{\eta}}(t) \tag{5.45}$$

$$\Omega^2\frac{\partial^2\mathbf{u}^2(\beta,t)}{\partial\beta^2}=\Omega^2\mathbf{A}^{21}\frac{\partial^2\mathbf{\Phi}^1_{rf}(\beta)}{\partial\beta^2}\boldsymbol{\eta}(t) \tag{5.46}$$

And again substituting this in (5.42) leads to:

$$\begin{aligned}
&\mathbf{M}^2_{rf}\mathbf{A}^{21}\mathbf{\Phi}^1_{rf}(\beta)\ddot{\boldsymbol{\eta}}(t)+2\mathbf{M}^2_{rf}\left(\hat{\mathbf{\Omega}}\mathbf{A}^{21}\mathbf{\Phi}^1_{rf}(\beta)+\Omega\mathbf{A}^{21}\frac{\partial\mathbf{\Phi}^1_{rf}(\beta)}{\partial\beta}\right)\dot{\boldsymbol{\eta}}(t)+\\
&\mathbf{M}^2_{rf}\left(\hat{\mathbf{\Omega}}^2\mathbf{A}^{21}\mathbf{\Phi}^1_{rf}(\beta)+2\Omega\hat{\mathbf{\Omega}}\mathbf{A}^{21}\frac{\partial\mathbf{\Phi}^1_{rf}(\beta)}{\partial\beta}+\Omega^2\mathbf{A}^{21}\frac{\partial^2\mathbf{\Phi}^1_{rf}(\beta)}{\partial\beta^2}\right)\boldsymbol{\eta}(t)+\\
&\mathbf{K}^2_{rf}\mathbf{A}^{21}\mathbf{\Phi}^1_{rf}(\beta)\boldsymbol{\eta}(t)=\mathbf{F}^2(t)
\end{aligned} \tag{5.47}$$

Finally transforming back to the reference coordinates and pre-multiplying by $\mathbf{\Phi}^{1T}_{rf}(\beta)$ leads to (keeping in mind that $\mathbf{M}^2_{rf}=\mathbf{A}^{21}\mathbf{M}^1_{rf}\mathbf{A}^{12}$ and $\mathbf{A}^{12}\hat{\mathbf{\Omega}}\mathbf{A}^{21}=\hat{\mathbf{\Omega}}$):

$$\begin{aligned}
&\ddot{\boldsymbol{\eta}}(t)+2\mathbf{\Phi}^{1T}_{rf}(\beta)\mathbf{M}^1_{rf}\left(\hat{\mathbf{\Omega}}\mathbf{\Phi}^1_{rf}(\beta)+\Omega\frac{\partial\mathbf{\Phi}^1_{rf}(\beta)}{\partial\beta}\right)\dot{\boldsymbol{\eta}}(t)+\\
&\mathbf{\Phi}^{1T}_{rf}(\beta)\mathbf{M}^1_{rf}\left(\hat{\mathbf{\Omega}}^2\mathbf{\Phi}^1_{rf}(\beta)+2\Omega\hat{\mathbf{\Omega}}\frac{\partial\mathbf{\Phi}^1_{rf}(\beta)}{\partial\beta}+\Omega^2\frac{\partial^2\mathbf{\Phi}^1_{rf}(\beta)}{\partial\beta^2}\right)\boldsymbol{\eta}(t)+\\
&\mathbf{V}\boldsymbol{\eta}(t)=\mathbf{\Phi}^{1T}_{rf}(\beta)\mathbf{F}^1(t)
\end{aligned} \tag{5.48}$$

Now define:

$$\mathbf{\Phi M}\partial\mathbf{\Phi}=\mathbf{\Phi}^{1T}_{rf}(\beta)\mathbf{M}^1_{rf}\left(\hat{\mathbf{\Omega}}\mathbf{\Phi}^1_{rf}(\beta)+\Omega\frac{\partial\mathbf{\Phi}^1_{rf}(\beta)}{\partial\beta}\right) \tag{5.49}$$

$$\mathbf{\Phi M}\partial^2\mathbf{\Phi}=\mathbf{\Phi}^{1T}_{rf}(\beta)\mathbf{M}^1_{rf}\left(\hat{\mathbf{\Omega}}^2\mathbf{\Phi}^1_{rf}(\beta)+2\Omega\hat{\mathbf{\Omega}}\frac{\partial\mathbf{\Phi}^1_{rf}(\beta)}{\partial\beta}+\Omega^2\frac{\partial^2\mathbf{\Phi}^1_{rf}(\beta)}{\partial\beta^2}\right) \tag{5.50}$$

And the system can be written in state space:

$$\begin{bmatrix} \dot{\boldsymbol{\eta}}(t) \\ \ddot{\boldsymbol{\eta}}(t) \end{bmatrix} = \begin{bmatrix} \mathbf{0} & \mathbf{I} \\ -\boldsymbol{\Phi}\mathbf{M}\partial^2\boldsymbol{\Phi} - \mathbf{V} & -2\boldsymbol{\Phi}\mathbf{M}\partial\boldsymbol{\Phi} \end{bmatrix} \begin{bmatrix} \boldsymbol{\eta}(t) \\ \dot{\boldsymbol{\eta}}(t) \end{bmatrix} + \begin{bmatrix} \mathbf{0} \\ \boldsymbol{\Phi}_{rf}^{1T}(\beta)\mathbf{F}^1(t) \end{bmatrix} \tag{5.51}$$

5.6 Discussion

It has been shown that it is necessary to use reference frame fixed modes to model the behaviour of the tyre correctly when an asymmetry in the modes is present (e.g. caused by initial deformation). These modes are constant in the reference frame, but rotate along with the excitation in the body fixed frame. One can describe the system in the body fixed coordinate system as well as in the reference coordinate system. The latter approach has several advantages over the one used in section 5.4:

- Φ_{rf}^1 is constant which means that no derivatives have to be determined at every time step.
- There is no interpolation necessary which improves accuracy.
- Because there is no interpolation necessary anymore, the ring or tyre does not have to be equally discretisized along the circumference. It can have a finer mesh near the contact patch.
- When calculating the response due to a roughness profile only the points likely to come into contact with the road have to be taken into account. The total response can be calculated afterwards.
- The response in this reference frame can be used directly to perform a sound radiation analysis.

A remark also has to be made however. Because the initial idea is to let the force rotate around the tyre instead of rotating the tyre itself, the stiffening of the tyre due to the rotation is not considered in this approach. This is not considered a problem as this effect is negligible in comparison to the stiffening due to inflation (see [Kim and Bolton, 2003]).

5.7 Contact model

The contact model that is used, is the elastic foundation model (or Winkler bedding, see [Johnson, 1985]) that is also used by Kropp [Kropp, 1999]. However there is a slight difference. In the Chalmers model the stiffness of the elastic foundation represents the tread stiffness. In our model this is incorporated in the modal base, so the stiffness represents the stiffness of the road. Furthermore some assumptions are made:

- Contact forces are always ”positive”. No tensile forces between the road and the tyre can exist.
- A force can only act on a point when it is in contact with the road.

In this thesis a difference is made between the static and dynamic situation. In the static situation an iterative procedure is used to determine the nodes that are in contact and the forces acting on them. Because the main goal of this thesis is to develop a vibration model of the tyre and not a contact model this iteration is not implemented (yet) in the dynamic situation.

5.7.1 Static

By using the modes and eigenvalues determined in the eigenvalue analysis a transfer function $H(\omega)$ can be defined (see [de Kraker, 2000]):

$$\mathbf{u}(t) = \mathbf{H}(\omega)\mathbf{f}(t) \tag{5.52}$$

and

$$\mathbf{H}(\omega) = \sum_{n=1}^{N} \left[\frac{\phi_n \phi_n^T}{\omega_n^2 - \omega^2} \right] \tag{5.53}$$

which simplifies to:

$$\mathbf{H}(0) = \mathbf{\Phi}_{bf}^2 \mathbf{V}^{-1} \mathbf{\Phi}_{bf}^{2T} \tag{5.54}$$

for the static case. Here $\mathbf{V}$ is the diagonal matrix containing the eigenvalues (ω_k^2). If an elastic foundation is assumed so that $\mathbf{f} = k(\mathbf{x}_0 + \mathbf{u} - \mathbf{r})$, where $\mathbf{r}$ is the road, k the foundation stiffness and $\mathbf{x}_0$ are the coordinates of the undeformed tyre, an iterative scheme can be made:

Step 1: Calculate $(\mathbf{x}_0 + \mathbf{u} - \mathbf{r})$ and determine which nodes are in contact.
Step 2: Determine submatrix $\mathbf{H}_i$ of $\mathbf{H}$ for the points in contact at iteration i.
Step 3: Calculate a new $\mathbf{f}_i$ using :

$$\begin{aligned} \mathbf{f}_i &= k(\mathbf{x}_0 + \mathbf{u} - \mathbf{r}) \\ \mathbf{f}_i &= k(\mathbf{x}_0 + \mathbf{H}_i \mathbf{f}_i - \mathbf{r}). \\ \mathbf{f}_i &= (\mathbf{I} - k\mathbf{H}_i)^{-1} k(\mathbf{x}_0 - \mathbf{r}). \end{aligned}$$

Step 4: Calculate new $\mathbf{u}$: $\mathbf{u}_i = \mathbf{H}\mathbf{f}_i$.
Step 5: Check for convergence: $|\mathbf{f}_i - \mathbf{f}_{i-1}| < tol$. If not satisfied return to step 1.

5.7.2 Stationary rolling

This is the same as in the static situation only now with:

$$\mathbf{H} = \mathbf{\Phi}_{\boldsymbol{rf}}^{\mathbf{1}} \left(\mathbf{\Phi} \mathbf{M} \partial^2 \mathbf{\Phi} + V \right)^{-1} \mathbf{\Phi}_{\boldsymbol{rf}}^{\mathbf{1T}} \tag{5.55}$$

5.7.3 Dynamic

For the dynamic simulation the iteration and determination of $\mathbf{H}$ are not implemented. For the dynamic simulation the contact forces are determined every time-step. One simply uses $\mathbf{f} = k(\mathbf{x}_0 + \mathbf{u} - \mathbf{r})$ to determine the forces and then removes the tensile forces. These tensile forces mean that those nodes are not in contact. Of course this means that the physical displacements $\mathbf{u}$ have to be determined by $\mathbf{u} = \mathbf{\Phi}_{rf}^1 \boldsymbol{\eta}$ at every time step.

5.8 Implementation

The approach using rotating modes and aforementioned contact model are implemented in Matlab. Only the 2D case is discussed here. However the 3D situation does not differ much from the 2D situation and can easily be derived from the 2D files. In the 2D case a circular ring is modelled in Abaqus. The data from the eigenvalue analysis in Abaqus is stored in an ASCII file. A Matlab program was written to extract the relevant data from this ASCII file (like node numbers, eigenvalues, modes etc.) and store it in the structure ”model”. This structure is used throughout the analysis. The m-files which are mentioned in this section can be found in appendix A.

run file.m

In this file the relevant model-file is loaded and variables are declared. Then the spatial derivatives of the modes are determined (spat der.m). Next $\mathbf{\Phi M}\partial\mathbf{\Phi}$ and $\mathbf{\Phi M}\partial^2\mathbf{\Phi}$ are determined using "rotating modes.m". Finally the transient analysis is performed and the results are plotted.

spat der.m

In this file the first and second spatial derivative with respect to angle β are determined. This is done by numerical differentiation along the circumference of the ring.

model dv all.m

This is the file containing the system of ode's to be solved by ode45. First the excitation forces $\mathbf{f}(t)$ resulting from the contact are determined using "con force.m". Then the system of ode's (5.51) to be solved is defined.

rotating modes.m

In this file $\mathbf{\Phi M}\partial\mathbf{\Phi}$ and $\mathbf{\Phi M}\partial^2\mathbf{\Phi}$ are determined as in (5.49) and (5.50) respectively.

con force.m

In this file the forces due to the elastic foundation are determined. The physical coordinates of the nodes are determined by adding the physical displacements $\mathbf{u}t$ to the base coordinates. Then the contact forces are determined using $\mathbf{f} = k(\mathbf{x}_0 + \mathbf{u} - \mathbf{r})$. Now points which are not in contact lead to tensile forces. These forces are thus removed from the force vector $\mathbf{f}(t)$.

y con func.m

This file contains the information on the constraint $\mathbf{r}$.

Chapter 6

Validation

In this chapter the theory from the previous chapter is validated. For this purpose a 2D ringmodel is used. The results from calculations in the body fixed frame are compared to calculations in the reference frame. Also the contact model is combined with the 2D model for some static simulations. Next the 3D model is used to and its eigenvalues for several rolling speeds are determined to see whether it also complies with (3.8). Finally a detailed FE model of a real tyre is compared to measurements which have been done in an earlier stage.
First of all however the two FE models which are used in this chapter are discussed briefly.

6.1 Validation models

As mentioned two models are used in this chapter. A 2D as well as a simple 3D model is used. This 3D model is not the same as used in chapter 4. The 2D model is a ring model. This ring is modelled in Abaqus using beam elements. (See figure 6.1). The parameters of this model are not all realistic parameters for tyres. This is not a problem however because the model is only used to test the theory. The parameters which are used can be found in appendix B. The cross-section of the 3D model is also shown in figure 6.1. Again the parameters can be found in appendix B.

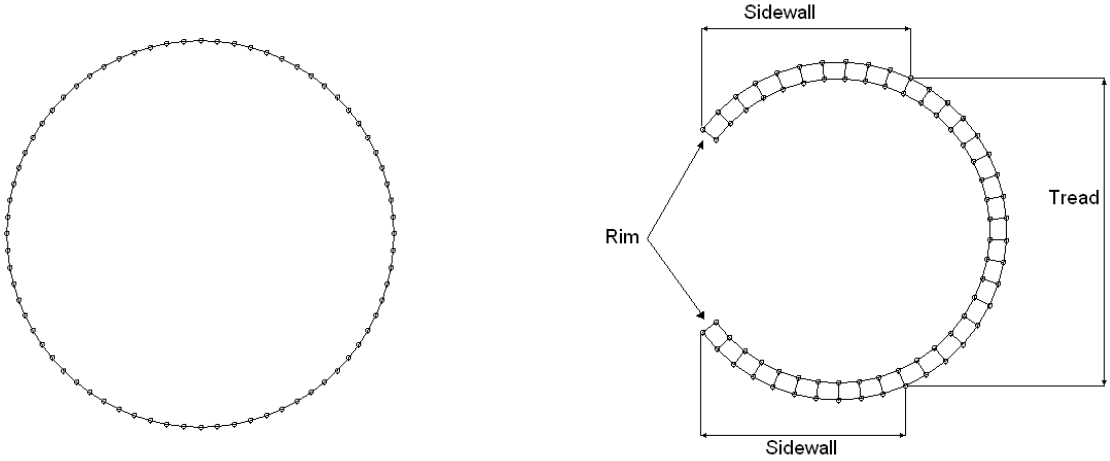

Figure 6.1: ***Left****: The FE model of the ring. Here shown with only 72 beam elements.* ***Right****: Cross section 3D FE model.*

6.2 The 2D ring model

6.2.1 Theory validation

To validate the theory with the reference frame fixed modes from section 5.5 an analytical description of the 2D ring is used. From theory (e.g. [Blevins, 1979]) it is known that the radial displacements of the modeshapes of a ring look like $u = cos(n\alpha)$ and $u = sin(n\alpha)$. Here n is the number of waves along the circumference.
These analytical modes are used to calculate the eigenvalues in the body fixed frame (from (5.34)) and in the reference frame (from (5.51)). Also the response to a sinusoidal excitation is compared for both approaches. In the body fixed frame the body fixed mode shapes are written as:

$$\mathbf{\Phi}^2_{bf} = \begin{pmatrix} cos(n\alpha) & sin(n\alpha) \end{pmatrix} \tag{6.1}$$

And $\mathbf{\Phi}^1_{rf}$ is:

$$\mathbf{\Phi}^1_{rf} = \begin{pmatrix} cos(n\beta) & sin(n\beta) \end{pmatrix} \tag{6.2}$$

Diagonal matrix $\mathbf{V}$ belonging to these modes is:

$$\mathbf{V} = \begin{pmatrix} \omega_n^2 & 0 \\ 0 & \omega_n^2 \end{pmatrix} \tag{6.3}$$

where ω_n is the eigenfrequency belonging to the modes. We can now write the equations in state space form as in (5.34). Now define $\mathbf{B}^2_{bf}$ as:

$$\mathbf{B}^2_{bf} = \begin{pmatrix} \mathbf{0} & \mathbf{I} \\ -\mathbf{V} & \mathbf{0} \end{pmatrix} \tag{6.4}$$

Now the eigenvalues of in the fixed body frame can be determined by:

$$det(\lambda\mathbf{I} - \mathbf{B}^2_{bf}) = 0 \tag{6.5}$$

Leading to the (obvious) eigenvalues: $\lambda = \begin{pmatrix} j\omega & j\omega & -j\omega & -j\omega \end{pmatrix}$ Now, by using (5.51), we get:

$$\ddot{\boldsymbol{\eta}}(t) + 2\Omega \begin{pmatrix} 0 & n \\ -n & 0 \end{pmatrix} \dot{\boldsymbol{\eta}}(t) + (\mathbf{V} - n^2\Omega\mathbf{I})\eta(t) = \mathbf{\Phi}^{1T}_{rf}\mathbf{F}^1 \tag{6.6}$$

And $\mathbf{B}^1_{rf}$ can be defined as:

$$\mathbf{B}^1_{rf} = \begin{pmatrix} \mathbf{0} & \mathbf{I} \\ n^2\Omega^2\mathbf{I} - \mathbf{V} & -2\Omega \begin{pmatrix} 0 & n \\ -n & 0 \end{pmatrix} \end{pmatrix} \tag{6.7}$$

Leading to the eigenvalues: $\lambda = \begin{pmatrix} j(\omega - n\Omega) & j(\omega + n\Omega) & -j(\omega - n\Omega) & -j(\omega + n\Omega) \end{pmatrix}$ Which clearly shows the splitting of the eigenvalues.
Next a sinusoidal force is applied:

$$\mathbf{F}^1(t) = F\delta(\beta)cos(\omega t) \tag{6.8}$$

$$\mathbf{F}^2(t) = F\delta(\alpha + \Omega t)cos(\omega t) \tag{6.9}$$

The parameters that are used are:

$$\mathbf{V} = \begin{bmatrix} 37.73 & 0 \\ 0 & 37.73 \end{bmatrix}, n = 2, F = 1N, \omega = 10rad/s, \Omega = 10rad/s$$

These parameters match the ones form the FE ring model so the results can be compared. In figure 6.2 the radial response of the point on the ring at $\alpha = 0$ in the body fixed frame is shown for four situations:

1. Analytic with body fixed modes
2. Analytic with reference frame fixed modes
3. Numerical with reference frame fixed modes
4. Numerical with body fixed modes

Here analytic means that the modes from (6.1) and (6.2) are used, leading to the system in (6.6) for the reference frame fixed modes. The response is determined with the Symbolic Toolbox of Matlab. For the numerical simulations, the modes of the 2D ring model are determined in Abaqus and the Matlab implementation discussed at the end of chapter 5 is used to determine the response. For the analytic

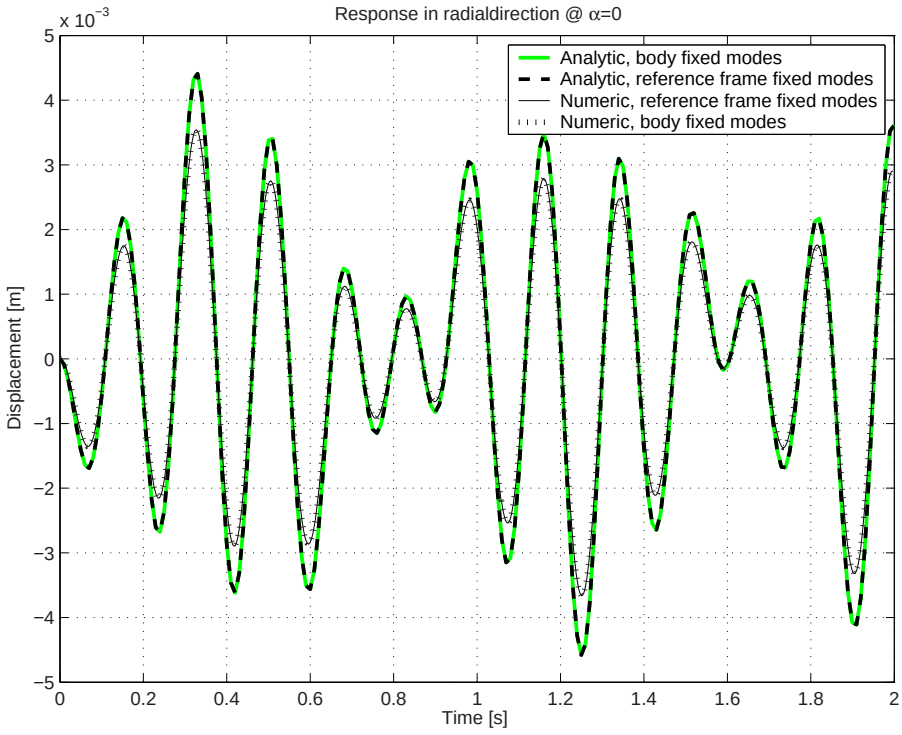

Figure 6.2: Response of the ring model.

as well as the numerical results there is no difference between the responses when using body fixed modes or reference frame fixed modes. This means that the theory and the implementation in Matlab are correct. There is a difference between the analytic results and the numerical results however, which is probably caused by the fact that the modes from the FE model are not purely radial modes as assumed in the analytic case but also have a tangential component.

6.2.2 Doppler-effect

As discussed in chapter 4 the rotation of the tyre leads to a shift of the dispersion curves. This effect is important and therefore should also be properly reproduced. In the previous section it has been shown that the eigenvalues are shifted due to the rotation. The effect of this on the dispersion curves is shown in this section. Normally the rotational velocity should remain below the first eigenfrequency or else the system would become unstable. This can be easily seen in (6.6) where the ”stiffness”-matrix ($\mathbf{V} - n^2\Omega\mathbf{I}$) would contain negative values. The ring model has such a low first eigenfrequency that the difference in dispersion characteristics would be difficult to see. To overcome this problem the first and second eigenfrequency are left out for the purpose of this calculation. The FRF's from the point at $\beta = 0$ to all other points on the ring are determined. This is done for the frequency range 100-1000 Hz. (See figure 6.3). Then for each frequency for which the steady state response is calculated, a

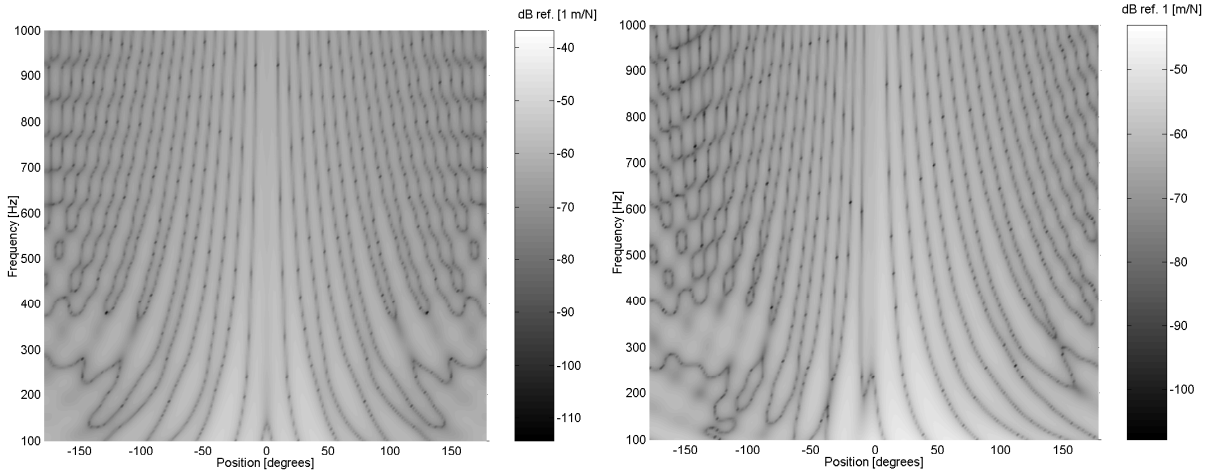

Figure 6.3: FRF of the ring model. ***Left:****FRF Amplitudes for* $\Omega = 0$.***Right:*** *FRF Amplitudes for* $\Omega = 30\pi rad/s$.

spatial FFT is performed which leads to the dispersion plots in figure 6.4 The square symbols in the

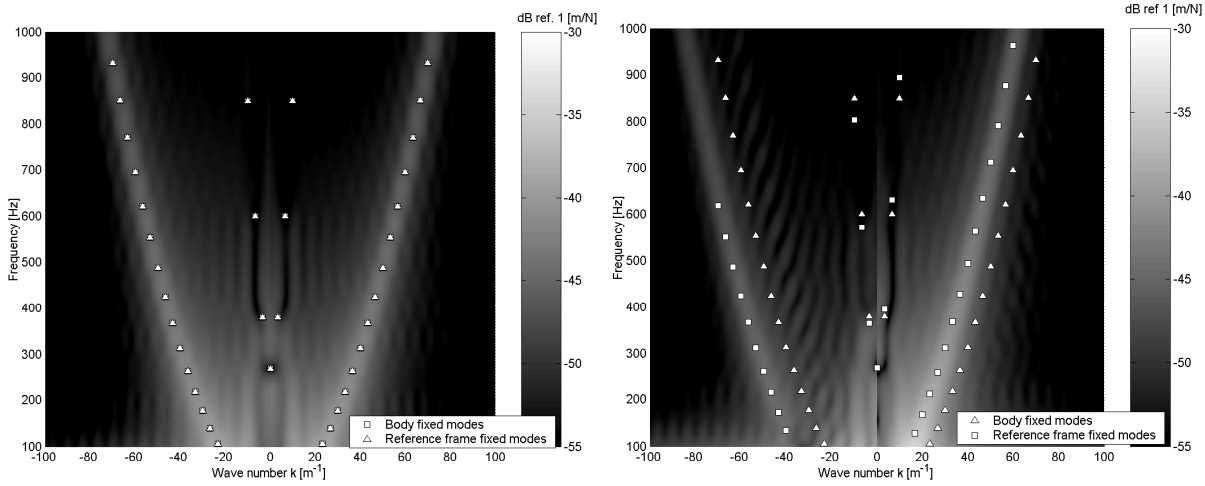

Figure 6.4: Dispersion characteristics of the ring model. ***Left:*** *Dispersion curves for* $\Omega = 0$.***Right:*** *Dispersion curves for* $\Omega = 30\pi rad/s$.

figures indicate the eigenfrequencies determined in the eigenvalue analysis for $\Omega = 0$. The triangular symbols are the corrected eigenvalues using the equation of Kim and Bolton (3.8). The right figure clearly shows that the response calculated using modal superposition satisfies this equation.

6.2.3 The contact model

In this section some results for the contact model in combination with the 2D model are shown. Again the results from calculations in Matlab are compared to calculations done in Abaqus. This has been done for the static (non-rotating) situation only. The main interest for doing these comparisons is to find out how important the influence of the number of modes is in comparison to the stress variations in the material due to the contact (the effect described in chapter 4). To do this one Abaqus simulation using the 2D model is done and compared to calculations in Matlab using a different number of modes each time. Figure 6.5 shows the deformation of the ring when the constraint (road) is moved up 0.05m. In the top figure in figure 6.6 the total contact force for different number of modes is shown. In the

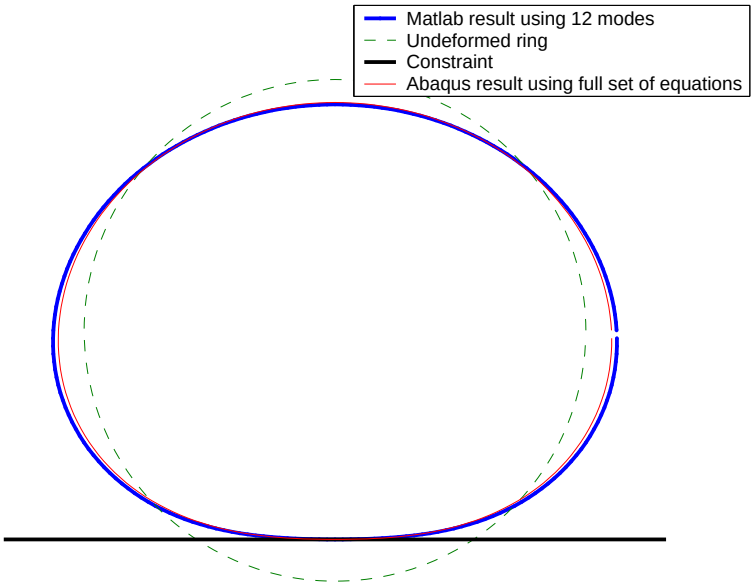

Figure 6.5: Deformation of the ring due to contact.

lower figure the relative error in comparison to the result from Abaqus is shown. One can clearly see that when using a small number of modes the error is large, but it reduces rapidly when the number of modes is increased. However from about 10-15 modes there is no difference noticeable anymore. The remaining error is caused by the fact that the effect described chapter 4 is not taken into account because the modes were determined in the undeformed situation. This is supported by the observation that the relative error decreases when the constraint is moved 0.01m instead of 0.05m. Because the deformation is larger, the influence in the stiffness is also more important. These results again clearly show that the modes have to be determined in the deformed situation.

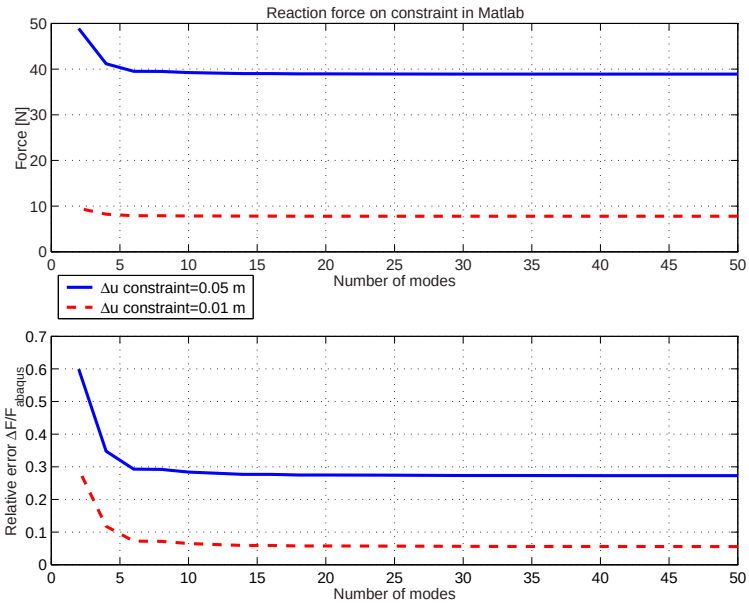

Figure 6.6: Comparison of total contact force in Matlab ⇔ Abaqus

6.3 The 3D model

In the previous sections the theory from chapter 5 has been verified with use of a 2D ring model. In the section an attempt is made to validate the approach for a 3D model that is combined with the contact model from section 5.7. But first it is shown that for the 3D model the splitting of frequencies also occurs.

6.3.1 Doppler effect

Figure 6.7 (**Left**) shows the frequency response functions of the 3D model for a rotational velocity of 0 rad/s and 100 rad/s. In the figure the 1 indicates the mode with n=1 and m=1 (see figure 2.1). The 1* indicates the two modes which are created when the tyre is rotating. These modes are shifted $\pm\frac{100}{2\pi} \approx \pm 16$ Hz with respect to the situation where $\Omega = 0$rad/s. 2 and 2* indicate the mode with n=2 and m=1 for the non-rotating and rotating tyre respectively. The latter are shifted $\pm 2\frac{100}{2\pi} \approx \pm 32$Hz. 3 indicates the the mode with n=0 and m=1. This mode does not shift due to the rotation as there is no variation of this mode along the circumference. This effect is also shown in the right figure in figure 6.7. In this figure the eigenvalues corresponding with the 10 first eigenmodes (in the non-rotating situation) are shown. These are determined from the matrix in (5.51). Again the splitting of the eigenvalues can be seen. Some numerical values are given in table 6.1. The steepness of the lines is determined by the number of wavelengths along the circumference (or the wave number k_ϕ) as in (3.8).

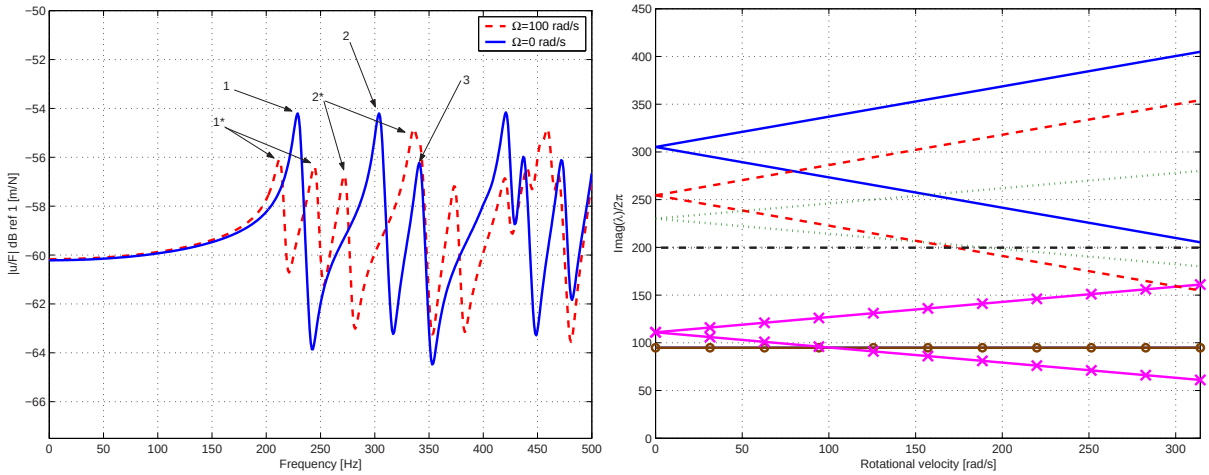

*Figure 6.7: **Left**: Point admittance of the 3D model for $\Omega = 0 rad/s$ and $\Omega = 100 rad/s$. **Right**: Eigenvalues of the first 10 modes for different Ω's*

$\Omega \rightarrow$	0	20π	40π	60π	80π	100π
$\text{imag}(\lambda_1)/2\pi$	94.8	94.8	94.8	94.8	94.8	94.8
$\text{imag}(\lambda_2)/2\pi$	111.0	101.0	91.0	81.0	71.0	61.0
$\text{imag}(\lambda_3)/2\pi$	111.0	121.0	131.0	141.0	151.0	161.0
$\text{imag}(\lambda_4)/2\pi$	199.6	199.6	199.6	199.6	199.6	199.6
$\text{imag}(\lambda_5)/2\pi$	230.1	220.1	210.1	200.1	190.1	180.1
$\text{imag}(\lambda_6)/2\pi$	230.1	240.1	250.1	260.1	270.1	280.1
$\text{imag}(\lambda_7)/2\pi$	254.5	234.5	214.6	194.6	174.7	154.7
$\text{imag}(\lambda_8)/2\pi$	254.5	274.5	294.4	314.4	334.3	354.3
$\text{imag}(\lambda_9)/2\pi$	305.1	285.2	265.2	245.2	225.3	205.3
$\text{imag}(\lambda_{10})/2\pi$	305.1	325.1	345.1	365.0	385.0	405.0

Table 6.1: Eigenvalues of the first 10 modes for different Ω's

6.3.2 Validation

The first comparison that is made includes the contact model described in chapter 5. The constraint (the road) is moved up and down with a sinusoidal displacement of frequency 20 Hz and amplitude 5 mm. So roughly from 0 - 5mm there is contact and from -5mm - 0mm there is no contact. This has been done for a non-rotating tyre and a tyre that rotates with 100 rad/s. The stiffness of the springs in the elastic bedding is chosen rather low at 10 kN/m. Clearly the Abaqus data has to be transformed from the local, body fixed coordinate system to the reference system, leading to errors due to interpolation. The displacement of the point in the center of the contact patch for these analyses is shown in figure 6.8. It can be seen that the results differ especially in the region where the displacement due to the contact is the largest. There are several reasons for this: the modes of the tyre are determined in the undeformed situation and the contact model may also cause differences as the model implemented in Matlab uses no iteration and the one in Abaqus does. Also it turns out that for the 3D model the

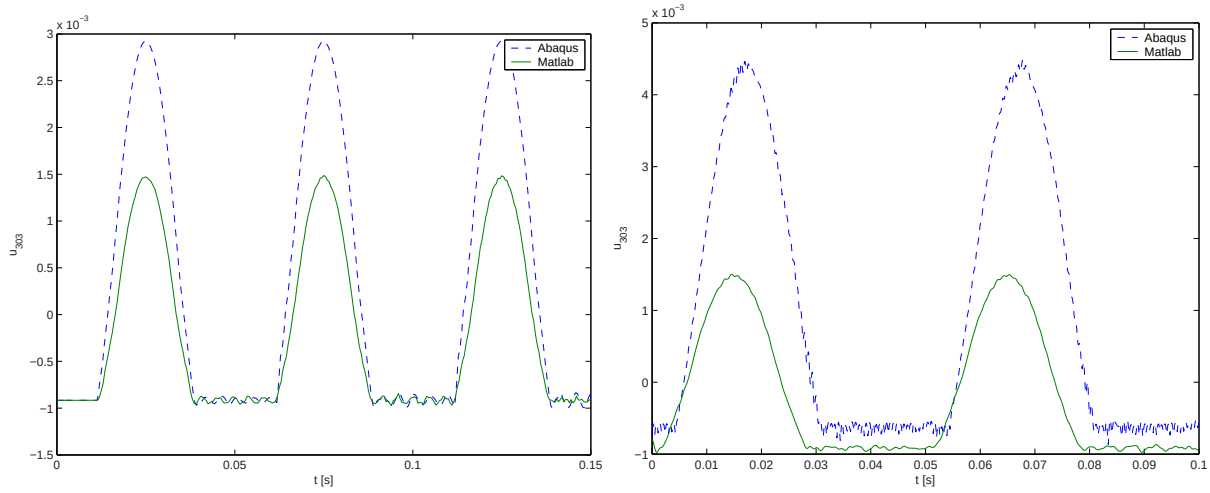

Figure 6.8: ***Left****: Time response for the non-rotating tyre.* ***Right****: Time response for the rotating tyre.*

influence of the number of modes on the accuracy is larger than in the 2D situation. For these simulations already 200 modes have been used. Another problem is that the forced response is too large to be able to distinguish the free response. In appendix C figure C.1 the FFT of the displacement of the aforementioned point for the non-rotating tyre can be seen. Here also the forced response is too dominant. The ”impulses” of the moving constraint every $1/20$ second lead to peaks in the spectrum every 20 Hz. This makes it impossible to distinguish other information in the spectrum. Therefore another approach is chosen.

In the second comparison the constraint is removed and so the contact model is not used anymore. Now a point force consisting of noise is applied at the center of the tread. Again for a rotating (20 Hz or 40*π rad/s this time) situation and a non-rotating situation. Then the point admittance is determined for both cases. See figure 6.9. In the non-rotating situation the results are similar. At least the resonance peaks show up at about the same frequencies. For the rotating situation on the other hand the result from Abaqus is not good at all. The results from Matlab at least show peaks at 210 and 250 Hz. (Peaks 1* from the left picture from figure 6.7 only shifted 20 Hz instead of 16.), but the peaks in the FRF calculated from the Abaqus results cannot be explained like this. This problem could be caused by the transformation from the local frame to the reference frame that is performed on the Abaqus data. To check this other, even more basic simulations are carried out.

Now the force that is applied is not longer a noise signal, but a pure sine, with a frequency of 230 Hz. Again this is done for a non-rotating and a rotating tyre. Figure 6.10 shows the FFT’s of the response of the point where the force is applied. In the non-rotating case the results are almost identical. It has to be mentioned however that Abaqus uses some sort of numerical damping to keep the simulation stable. The damping in Matlab is chosen such that the amplitude at 230 Hz is equal to the amplitude from Abaqus. However this damping may not be correct in other situation (e.g. when $\Omega > 0$). This is immediately confirmed by the right picture in figure 6.10. The frequency at which the peak appears on the other hand seems to match very good. But if one takes a closer look (see figure 6.11) it appears that a lot of peaks turn up at frequencies $230 \pm 20n$ Hz (where n=0,1,2,...,N-1,N

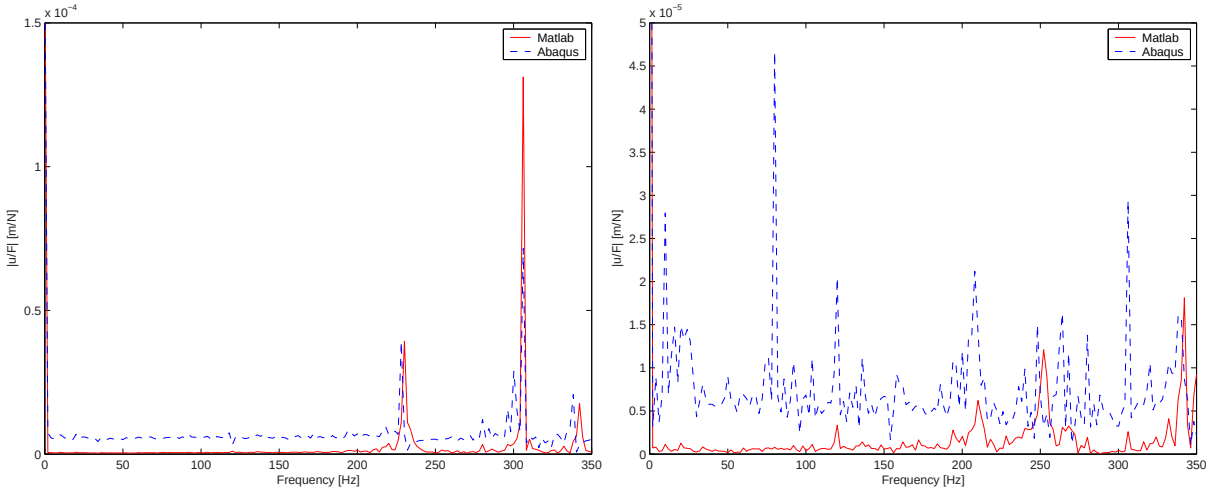

*Figure 6.9: **Left**: FRF for the non-rotating tyre. **Right**: FRF for the rotating tyre.*

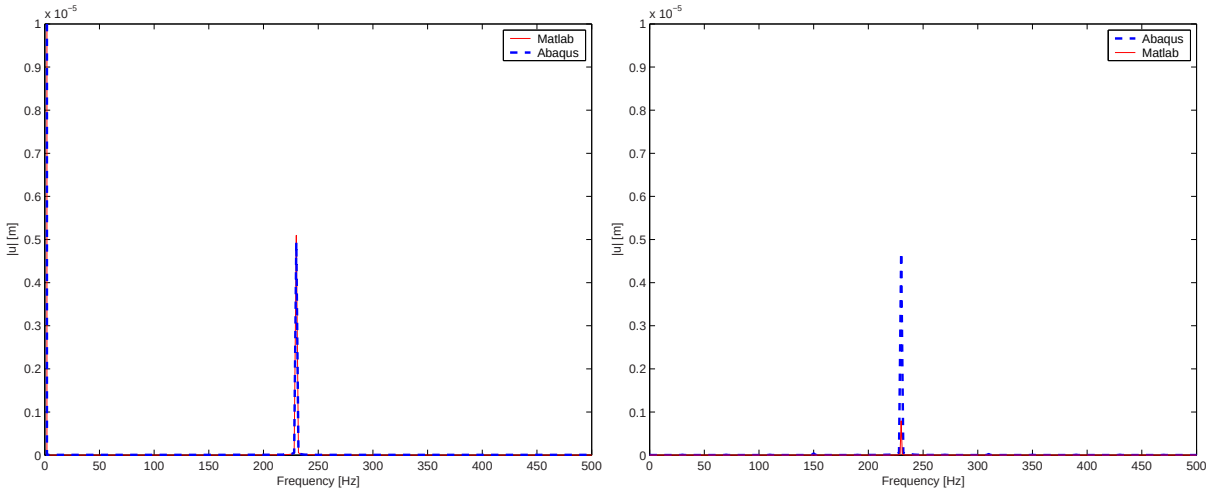

*Figure 6.10: **Left**: FFT for the non-rotating tyre. **Right**: FFT for the rotating tyre.*

and N is the maximum number of modal diameters in the modes included in the response). The explanation for this can be found in [Thompson, 1993]. Here it is shown that in the local, body fixed frame a force of frequency ω (which rotates around the tyre with Ω rad/s in this frame) leads to responses at frequencies $\omega \pm n\Omega$. The transformation to the reference frame should then eliminate these ”extra” peaks, but it appears that the transformation of the Abaqus results from the local frame to the reference frame leads to errors. There are two possible reasons for this:
1) The interpolation. Because the results from Abaqus are not computed with a fixed time step, one has to interpolate to be able to transform these results to the reference frame. This leads to errors which may be the cause that the peaks at $\omega \pm n\Omega$ do not disappear completely.
2) Aliasing. The time-step that is used in Abaqus is around 0.5 ms. This means that the sampling frequency is 2000 Hz and thus the highest frequency that can be detected is 1000 Hz. But because

the Abaqus model uses the full equations, modes with very high *n* numbers are present, leading to frequencies in the response higher than 1000Hz. Whichever of these 2 the main reason is, the problem clearly gets even worse when then excitation is not just one frequency but a noise signal. Because of this problem no good comparison can be made at the moment.

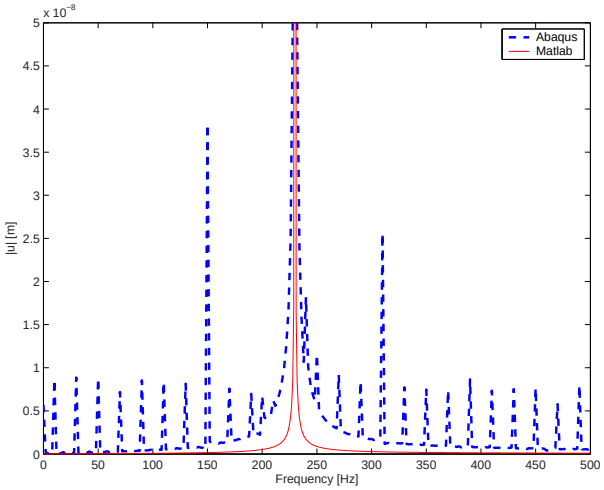

Figure 6.11: Close-up of the right picture of figure 6.10

6.4 Comparison of the Vredestein FE model to measurements

The validations done in this chapter with use of the model from figure 6.1 indicate that the theory is correct. However to be able to give a good prediction of the response of a tyre the FE model has to be a very good representation of the real tyre. In this section results from a rather detailed model of a real tyre is compared to measurements. These measurements are taken from [Blom, 2004]. The first comparison is a simple comparison between two frequency response functions (FRF). The tyre is excited in radial direction in a frequency range from 0-500 Hz. Figure 6.12 shows the results. It is clear that there is a large difference between measurement and calculation. The FRF of the FE model has a much larger amplitude than is measured. It seems that the stiffness of the model is much lower than in reality. This is also supported if one has a look at figure 6.13. All modes determined in the FE analysis appear at much lower frequencies than measured in the experiment, again indicating a stiffness that is too low. It turns out that it is very difficult to develop a quantitatively good FE model. This has several reasons:

- The material parameters have to be determined very accurately. However this is very difficult. E.g. the material stiffness is frequency dependent, which is not taken into account at the moment. Furthermore material damping is not included. For this analysis simple modal damping is used. Determining the correct material parameters is probably the biggest challenge in creating a good FE model
- The geometry of the tyre is very complicated. The tyre is made up from several layers which all have different properties. Not only the properties of these layers have to defined correctly, but also their location in the tyre. Another difficulty when modelling a tyre is the tread pattern.

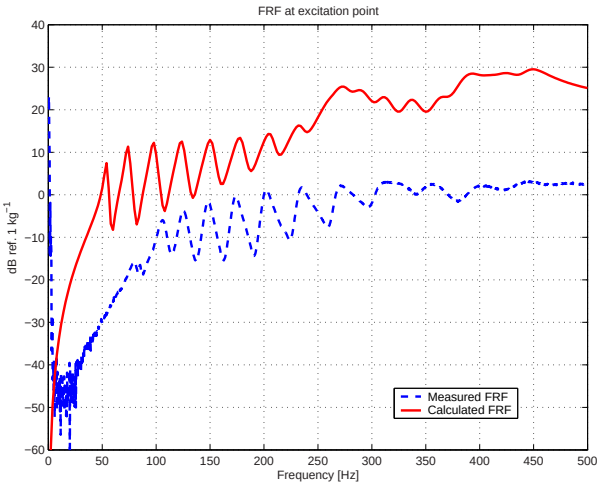

Figure 6.12: FRF of the tyre at the excitation point.Calculated and measured [Blom, 2004]

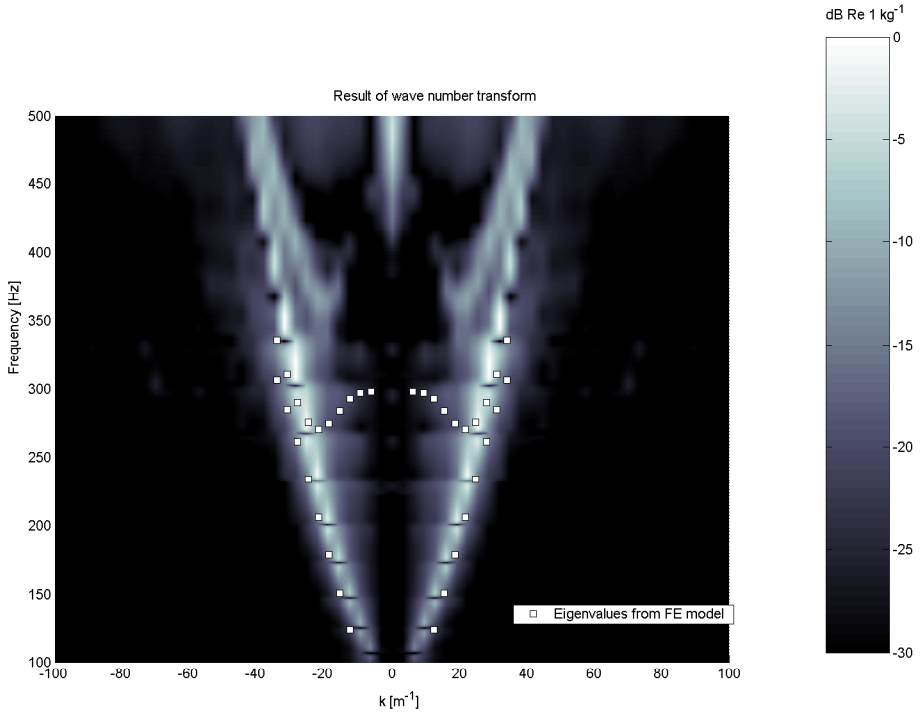

Figure 6.13: Dispersion of the Vredestein tyre [Blom, 2004]. The squares indicate the eigenfrequencies of the FE model

It is very difficult to model this correctly and in the current model, apart from a couple of circumferential grooves, the tread pattern is not included.

6.5 Discussion of the modelling approach

In the preceding chapter it has been shown that the theory from chapter 5 is correct. The results from calculations in the local coordinate system have been compared to calculations in the reference coordinate system and are found to be in good agreement. It has also been shown that this approach models the splitting of the eigenvalues due to the rotation of the tyre correctly, for the simple 2D situation as well as the more complex 3D situation. Furthermore by using the 2D model in combination with the contact model it has been pointed out once more that it is very important to take the initial deformation into account when calculating the eigenvalues. This is especially important for low frequencies. Not doing so will result in large errors later on. A drawback of the modelling approach is that a for the 3D case a large number of modes is required to reach a satisfying accuracy. However it is still expected that the simulation times can be reduced significantly, although it is rather difficult to say how much because this has not been investigated well enough. An example can be given though. For the simulation with the rotating sinusoidal excitation that has been discussed earlier in this chapter the Matlab simulation was 11 times faster than the Abaqus simulation. 100 modes have been used for the Matlab simulation. But this is in comparison with a very simple FE model (only 7600 nodes). The more complicated the FE model gets, the bigger the advantage of the modal approach. In addition to that Abaqus is a highly optimized package while the matlab implementation that has been used can probably be improved a great deal.
An attempt has also been made to validate the modal approach against simulations in Abaqus. However due to errors in postprocessing this attempt has not been successful. Furthermore a FE model of an actual tyre has been compared to measurements. The eigenvalues and a FRF for the non-rotating situation have been determined, leading to the conclusion that the FE model is not accurate enough at the moment.

Chapter 7

Conclusions and recommendations

7.1 Conclusions

During the literature study several modelling approaches have been found. However each approach has its own advantages and disadvantages. Main disadvantage of all analytical models is that they have smeared out material properties, which are difficult to determine. Another problem with most analytical models is that they are only valid in certain frequency ranges. Because of this it seems there is no model which is able to give good predictions in the 0-500 Hz region. For the semi-analytical approaches it is difficult to describe the contact with the road. Therefore determining the eigenvalues and eigenmodes of a detailed FE-model of the tyre and then using these to construct a modal base of the tyre seems a computationally cheap way of calculating the time-domain response of the tyre without neglecting its complex build-up. This approach has thus been further examined in this thesis.

In chapter 4 the behaviour of a tyre has been examined by using a FE model of a model tyre. Especially the influence of the contact with the road on the dynamic behaviour of the tyre has been investigated. It turns out that the stiffness of the tyre decreases near the contact patch due to a change in internal stress. This leads to a change in dynamic behaviour. Secondly the effect of the rotation on the dispersion curves has been shown for regular vehicle speeds. This shows that this effect is significant and has to be considered.

Taking the first effect into account is done by determining the modal base around the deformed state. The second effect is taken into account by describing the steady state rotation with an Eulerian approach. This makes it possible to determine the large stationary deformations with the full equations and possibly non-linear material properties, while the small, transient displacements are superposed on this state by using a limited number of modes. This approach has been derived in chapter 5 and a Matlab implementation has been made. Now the modes of a deformed tyre can be determined in Abaqus using the full model. Then these modes are exported to Matlab where the response of the rotating tyre can be determined. In addition to this a simple contact model is implemented for doing contact simulations.

An attempt to validate the approach from chapter 5 has been made in chapter 6, but because of problems in post processing the Abaqus results no satisfying comparison can be made between the results from Matlab and the results from Abaqus. On the other hand the remaining results, the dispersion plots and FRF's (e.g. figures 6.7 and 6.4), do not lead to doubts about this approach. These results

agree with results from literature (e.g. [Kim and Bolton, 2003] and [Thompson, 1993]) and therefore the approach is still thought to be correct. A drawback of the approach discussed in this thesis is that probably a large number of modes is needed to get accurate results. However it is still expected that the simulation times can be reduced significantly. Finally, a detailed model of an actual tyre has been compared to measurements in chapter 6. This shows that the FE model of the tyre is not good enough yet.

7.2 Recommendations

- The approach discussed in chapter 5 has been implemented. However some improvements can still be made. At the moment the implementation assumes an equidistant discretization along the circumference. But this is not necessary. By adjusting the m-file in which the spatial derivatives are calculated (spat_der.m) it is possible to use a finer mesh near the contact patch.
- When using the contact model, at the moment all points are considered when checking for contact. By selecting the points which are likely to come into contact with the road in advance, it is possible to take only those nodes into account. This will accelerate the calculations.
- At the moment a large number of modes is needed to get accurate results. However many of these modes do not contribute to sound generation. Developing a procedure to make a ”smart” choice from these modes may repair this problem. A ”smart” choice would mean using only those modes which are important for sound radiation or are necessary to describe the contact well.
- The contact model can be improved be adding an iterative procedure to it to determine the points that are in contact.
- The modelling approach still has to be validated. This should be done in two steps: first a comparison has to be made between calculations with Abaqus (using the ”full” system equations) and calculations using the modal approach discussed in this thesis. The most important problem here has been discussed in chapter 6: getting the transformation from local coordinates to reference coordinates correct. If these results are satisfactory the next step can be made where the numerical results are compared to measurement data of a rolling tyre.
- Chapter 6 shows that there is still a large difference between the FE model of the tyre and measurements performed on the same type of tyre. Therefore it is also necessary to improve this FE model.
- Until a good FE model is available it may also be possible to use experimentally determined modes of the (deformed) tyre in this approach. This would also be another way of validating this model.

Bibliography

R. D. Blevins. *Formulas for natural frequency and mode shape*. Van Nostrand Reinhold, London, 1979.

R. E. A. Blom. Report on tyre/road noise: Generation mechanisms, influence of tyre parameters and experiment on belt resonances. Technical Report DCT 2004.20, Technische Universiteit Eindhoven, 2004.

F. Boehm. Mechanik des guertelreifens. *Ing-Arch*, 35:82, 1966.

M. Brinkmeier. Finite elemente analyse der eigendynamik rollender rder. Master thesis, Institut fr Baumechanik und Numerische Mechanik,Universitt Hannover, 2003. Matrikel-Nr.1927700.

M. Brinkmeier, U. Nackenhorst, O. von Estorff, and S. Petersen. Physically based modelling of tire-rolling-noise by a finite element approach. In *Internoise 2004, Prague, Czech Republic, August 22-25*, 2004.

A. M. Burke and O. A. Olatunsbosun. Static tyre/road interaction modelling. *Meccanica*, 32:473–479, 1997.

B. de Kraker. *A Numerical and Experimental Approach in Structural Dynamics*. Technische Universiteit Eindhoven, 2000.

M. Eichler. Ride comfort calculations with adaptive tire models. In *AVEC'96 International symposium an advanced vehicle control, Aachen, 24-28 June*, 1996.

FTire. Ftire website. www.Ftire.com.

M. J. Gagen. Novel acoustic sources from squeezed cavities in car tires. *Journal of the acoustic Society of America*, 106(2):794–801, 1999.

S. Gong. *A study of in-plane dynamics of tires*. Phdthesis, Delft University of Technology,Faculty of mechanical engineering and marine technology, 1993.

R. A. G. Graf, C. Y. Kuo, A. P. Dowling, and W. R. Graham. On the horn effect of a tyre/road interface, part i: experiment and computation. *Journal of Sound and Vibration*, 256(3):417–431, 2002.

R. E. Hayden. Roadside noise from the interaction of a rolling tyre with the road surface. In *Proc. Of the Purdue Noise Control conference, Purdue University, Idiana, USA*, 1971.

M. Heckl. Tyre noise generation. *Wear*, 113:157, 1986.

K. L. Johnson. *Contact Mechanics*. Cambridge University Press, Cambridge,, 1985. ISBN 0 521 25576 7.

R. F. Keltie. Analytical model of the truck tire vibration sound mechanism. *Journal of the acoustic society of America*, 71(2):359–367, 1982.

P. Kessels. *Engineering toolbox for structural-acoustic design - Applied to MRI-scanners*. Phd thesis, Technische Universiteit Eindhoven, 2001.

Y. J. Kim and J. S. Bolton. Modeling tire treadband vibration. In *Proceedings of Internoise 2001 27-30 August, The Hague, Netherlands*, 2001.

Y. J. Kim and J. S. Bolton. Effects of rotation on the dynamics of a circular cylindrical shell with applications to tire vibration. *Journal of sound and vibration*, 275(3-5):605–621, 2003.

W. Kropp. Structure-borne sound on a smooth tyre. *Applied Acoustics*, 26:181–192, 1989.

W. Kropp. A mathematical model of tyre noise generation. *Heavy Vehicle Systems, Int. J. of Vehicle Design*, 6(1-4):310–329, 1999.

W. Kropp, K. Larsson, F. Wullens, P. Andersson, and F. X. Becot. The generation of tyre/road noise - mechanisms and models. In *ICSV 10 7-10 July 2003, Stockholm, Sweden*, 2003.

L. E. Kung. Radial vibrations of pneumatic radial tyres. *SAE Technical papers*, (900759), 1990.

K. Larsson and W. Kropp. A high-frequency three-dimensional tyre model based on two coupled elastic layers. *Journal of sound and vibration*, 253(4):889–908, 2002.

J. M. Muggleton, B. R. Mace, and M. J. Brennan. Vibrational response prediction of a pneumatic using an orthotropic two-plate wave model. *Journal of sound and vibration*, 264:929–950, 2003.

U. Nackenhorst. The ale-formulation of bodies in rolling contact: Theoretical foundations and finite element approach. *Computer Methods in Applied Mechanics and Engineering*, 193(39-41):4299–4322, 2004.

C.-M. Nilsson. *Waveguide finite elements applied on a car tyre*. Phd thesis, KTH, Stockholm, 2004.

C.-M. Nilsson and S. Finnveden. Tyre vibration analysis with conical waveguide finite elements. In *The 2002 International Congress and Exposition on Noise Control Engineering Dearborn, MI, USA. August 19-21*, 2002.

A. K. Noor, O. K. Kim, and J. A. Tanner. Analysis of aircraft tires via semi-analytic finite elements. *Finite elements in analysis and design*, 6:217–233, 1990.

D. J. O'Boy. Development of a tyre noise prediction model. Presentation at Department of Engineering, University of Cambridge, March 2004a.

D. J. O'Boy. Personal communication. e-mail with mr. O'Boy of University of Cambridge, March 4th 2004b.

R. J. Pinnington. Radial force transmission to the hub from an unloaded stationary tyre. *Journal of sound and vibration*, 253(5):961–983, 2002.

R. J. Pinnington and A. R. Briscoe. A wave model for a pneumatic tyre belt. *Journal of sound and vibration*, 253(5):941–959, 2002.

T. L. Richards. Finite element analysis of structural-acoustic coupling in tyres. *Journal of sound and vibration*, 149(2):235–243, 1991.

U. Sandberg. Tyre/road noise - myths and realities. In *Proceedings of the internoise 2001, the Hague, Netherlands*, 2001.

U. Sandberg and J. A. Ejsmont. *Tyre/road noise reference book*. Informex, SE-59040 Kisa, Sweden, 2002.

W. Soedel. On the dynamic response of rolling tires according to thin shell approximations. *Journal of sound and vibration*, 41:233–246, 1975.

R. Takagi and S. Takanari. Tire structural parameter analysis for road noise using an accurate fem model. *SAE Special Publications*, (911873), 1991.

D. J. Thompson. Wheel-rail noise generation, part v: inclusion of wheel rotation. *Journal of Sound and Vibration*, 161(3):467–482, 1993.

J. T. Tielking and R. A. Schapery. A method for shell contact analysis. *Computer methods in applied mechanics and engineering*, 26:181–195, 1981.

F. Wullens and W. Kropp. A three dimensional rolling contact model for the description of the tyre/road interaction. In *ICSV 10 7-10 July 2003, Stockholm, Sweden*, 2003.

Appendix A

M-file

A.1 run file.m

```
0001 close all; clear all;
0002 global U V F var model ds1U ds2U D base_co_full d
0003 %load data
0004 load('d:\documents_ron\m-files\mat-files\elas_circ.mat')
0005
0006 %enter variables
0007 var.Omega= 5*pi;                %Rotational velocity of the ring (rad/s)
0008                                  %!!!Caution!!! Has to smaller than 1st
0009                                  %eigenvalue
0010 var.nom=model.modes{end,1};     %Number of modes taken into account
0011 var.non=length(model.node_nr);  %total number of nodes
0012 var.nr_seg=length(model.el_nr); %total numer of segments
0013                                  %along circumference
0014 var.nps=1;                       %number of nodes per segment
0015 var.t_period=2*pi/var.Omega;    %time period of one rotation (s)
0016 var.t_record=[0:0.5e-3:1];      %time span for simulation (s)
0017 var.x_con=[-1:0.001:1];         %x values for constraint (m)
0018 var.K=1e5;                      %stiffness of elastic foundation springs (N/m)
0019
0020 %put base coordinates in a vector
0021 base_co_full=zeros(3*var.non,1);
0022 base_co_full(1:3:end)=model.base_co(:,1);
0023 base_co_full(2:3:end)=model.base_co(:,2);
0024 base_co_full(3:3:end)=model.base_co(:,3);
0025
0026 %load modes
0027 [var.U,var.V]=load_modes(model,var);
0028
0029 %Raleigh damping matrix
0030 D=0.2*model.mass_mat+0.0002*model.stiffness_mat;
0031 var.d=var.U'*D*var.U;
0032 %determine spatial derivative
0033 [ds1U,ds2U]=spat_der(var.U,var);
0034
0035 %determine UMdU and UMd2U
0036 [var.U,var.dU,var.d2U]=rotating_modes(0,var.U,ds1U,ds2U,var);
0037 var.UMdU=var.U'*model.mass_mat*var.dU;
0038 var.UMd2U=var.U'*model.mass_mat*var.d2U;
0039
```

```
0040 %clear obsolete variables
0041 clear ds1U ds2U
0042
0043 %calculate response using modal superposition
0044 %Initial values
0045 y0=zeros(2*var.nom,1);
0046 options = odeset('OutputFcn','odeprint','OutputSel',[1]);
0047 %Call to ordinary differential solver ode45
0048 [t,Y]=ode45('model_dv_all',t_record,y0,options);
0049 %calculate physical response
0050 u=var.U*Y(:,1:var.nom)';
0051
0052 %plot results
0053 for i=1:length(var.t_record)
0054     t=var.t_record(i);
0055     coor=base_co_full+y(:,i);
0056     plot(coor(1:3:end),coor(2:3:end),'.',coor(523),coor(524),'r.')
0057     hold on
0058     plot([var.x_con],[y_con_func(t)],'k');
0059     hold off
0060     axis([-0.4 0.4 -0.4 0.4])
0061     grid on
0062     drawnow
0063 end
```

A.2 spat der.m

```
0001 function [ds1U,ds2U]=spat_der(U,var)
0002 %angel between 2 segments
0003 dalpha=2*pi/var.nr_seg
0004
0005 ds1U=zeros(size(U));ds2U=zeros(size(U));
0006
0007 %calculate first spatial derivative
0008 ds1U(1:3:end,:)=diff([U(1:3:end,:);U(1,:)],1,1)/dalpha;
0009 ds1U(2:3:end,:)=diff([U(2:3:end,:);U(2,:)],1,1)/dalpha;
0010 ds1U(3:3:end,:)=diff([U(3:3:end,:);U(3,:)],1,1)/dalpha;
0011 %correct for shift due to diff
0012 ds1U=(ds1U+[ds1U(end-2:end,:); ds1U(1:end-3,:)])/2;
0013
0014 %calculate 2nd spatial derivative
0015 ds2U(1:3:end,:)=diff([ds1U(1:3:end,:);ds1U(1,:)],1,1)/dalpha;
0016 ds2U(2:3:end,:)=diff([ds1U(2:3:end,:);ds1U(2,:)],1,1)/dalpha;
0017 ds2U(3:3:end,:)=diff([ds1U(3:3:end,:);ds1U(3,:)],1,1)/dalpha;
0018
0019 %correct for shift due to diff
0020 ds2U=(ds2U+[ds2U(end-2:end,:); ds2U(1:end-3,:)])/2;
```

A.3 Model dv all.m

```
0001 function xdot=model_dv_all(t,x)
0002 global U V D y_con base_co_full var model ds1U ds2U d
0003
0004 %calculate physical displacements
0005 real_x=var.U*x(1:var.nom,1);
0006
```

```
0007 %determine forces acting on nodes in contact
0008 f_real=con_force(t,real_x);
0009
0010 %% the system of ode %%%%%%%%%%%%%%%%%%%%%%%%%%%%%%%%%%%%%%%%%%%%%%%%%%%%%%%%%%%%
0011 xdot=[zeros(var.nom) eye(var.nom);
0012      -(var.UMd2U+var.U'*D*var.dU+var.V) -(2*var.UMdU+var.d)]*x...
0013      +[zeros(var.nom,1);var.U'*f_real];
0014 %%%%%%%%%%%%%%%%%%%%%%%%%%%%%%%%%%%%%%%%%%%%%%%%%%%%%%%%%%%%%%%%%%%%%%%%%%%%%%%%%%%
```

A.4 Rotating modes.m

```
0001 function [U,dU,d2U]=rotating_modes(t,U,ds1U,ds2U,var)
0002 % variables needed in var: nr_seg, Omega, nps
0003
0004 %Determine dU %%%%%%%%%%%%%%%%%%%%%%%%%%%%%%%%%%%%%%%%%%%%%%%%%%%%%%%%%%%%%%%%%%%
0005 OMEGA=[0          var.Omega  0;
0006        -var.Omega 0          0;
0007        0          0          0];
0008
0009 dU=reshape(OMEGA*reshape(U,3,var.non*var.nom),3*var.non,var.nom)...
0010     +var.Omega*ds1U;
0011 %%%%%%%%%%%%%%%%%%%%%%%%%%%%%%%%%%%%%%%%%%%%%%%%%%%%%%%%%%%%%%%%%%%%%%%%%%%%%%%%%%%
0012
0013 % Determine d2U  %%%%%%%%%%%%%%%%%%%%%%%%%%%%%%%%%%%%%%%%%%%%%%%%%%%%%%%%%%%%%%%%
0014 d2U=reshape(OMEGA^2*reshape(U,3,var.non*var.nom)+2*var.Omega*OMEGA*...
0015     reshape(ds1U,3,var.non*var.nom),3*var.non,var.nom)...
0016       +var.Omega^2*ds2U;
0017 %%%%%%%%%%%%%%%%%%%%%%%%%%%%%%%%%%%%%%%%%%%%%%%%%%%%%%%%%%%%%%%%%%%%%%%%%%%%%%%%%%%
```

A.5 con force.m

```
0001 function f_real = con_force(t,real_x)
0002 global var base_co_full
0003
0004 coor_real=base_co_full+real_x;
0005
0006 %check for contact
0007 y_con_nodal=interp1(var.x_con,y_con_func(t),coor_real(1:3:end));
0008
0009 % determine forces due to contact
0010 f=-var.K*(coor_real(2:3:end)-y_con_nodal);
0011
0012 %Only positive (no tensile) forces
0013 cont_nodes=find(f<0);
0014 f(cont_nodes)=0;
0015
0016 %create full force vector
0017 f_real=zeros(600,1);
0018 f_real(2:3:end)=f;
```

A.6 y con func.m

```
0001 function y_con = y_con_func(t)
0002 global var
0003 %file containing the constraint the has to be satisfied
```

```
0004 if t<=0.1
0005     y_con = ones(size(var.x_con))*0.5*t

+0.1*t*sin(40*(var.x_con+0.25*var.Omega*t))-0.3;
0006 else
0007     y_con = ones(size(var.x_con))*0.5*0.1

+0.01*sin(40*(var.x_con+0.25*var.Omega*t))-0.3;
0008 end
```

Appendix B

Model parameters

The 2D model

Parameter	Definition	Value
a	Radius of the ring	0.3$[m]$
E	Elastic modulus of the ring material	$2 \cdot 10^9[N/m^2]$
ν	Poisson ratio of the ring material	0.3 [-]
ρ	Density of the ring material	7800 $[rad/s]$
r	Radius of the circular cross-section	0.005 $[m]$

The 3D model

Parameter	Definition	Value
a	Outer tyre radius	0.3$[m]$
d	Tread/Sidewall thickness	0.01 $[m]$
E_{tread}	Elastic modulus of the tread material	$4.8{\cdot}10^8[N/m^2]$
ν_{tread}	Poisson ratio of the tread material	0.45 [-]
E_{side}	Elastic modulus of the sidewall material	$4.8{\cdot}10^8[N/m^2]$
ν_{side}	Poisson ratio of the sidewall material	0.45 [-]
ρ	Density of the material	1200 $[rad/s]$
r	Outer radius of the circular cross-section	0.1 $[m]$

Appendix C

Figures

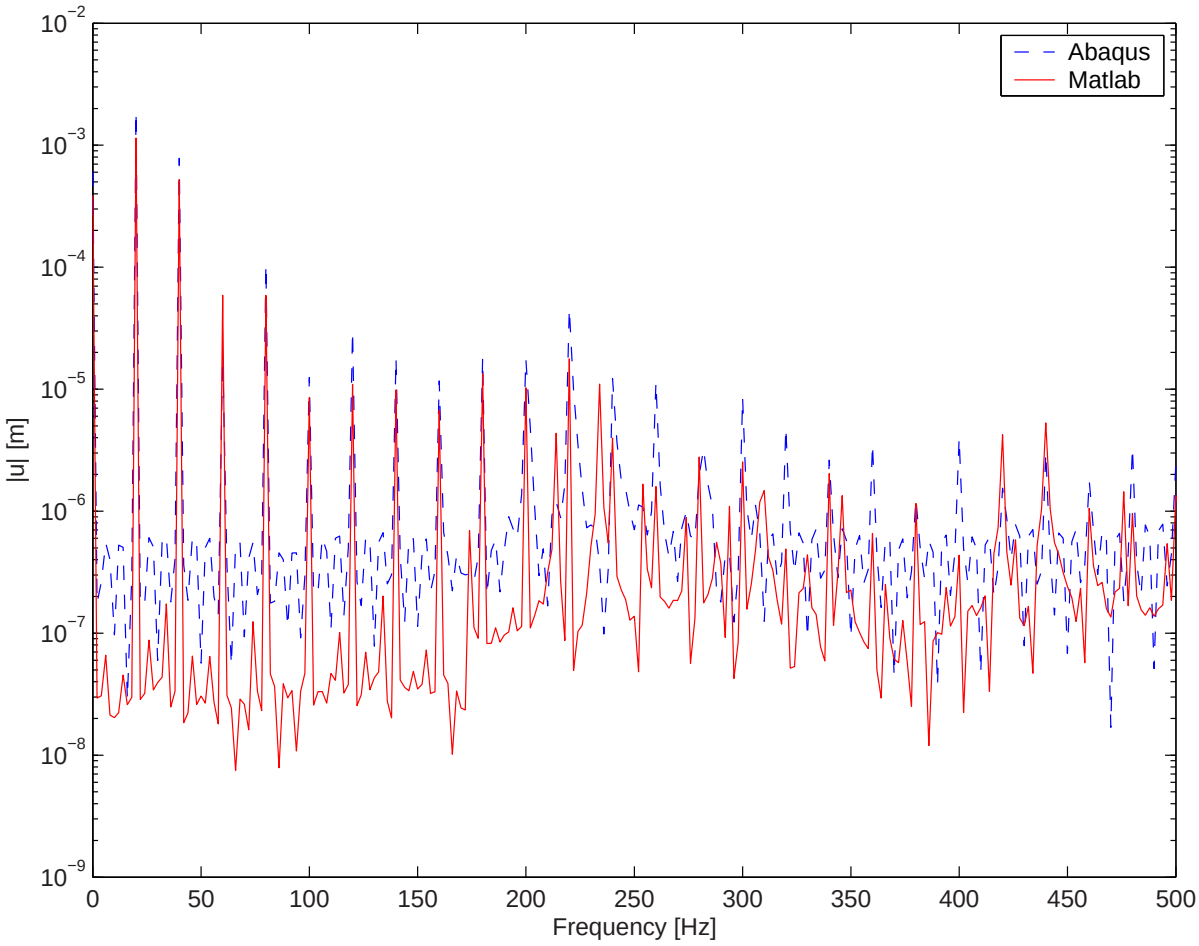

Figure C.1: FFT of the time response for the non-rotating tyre.